# Comparison of Convection-Permitting and Coarser-Resolution Regional Climate Simulations for Evaluating Precipitation and Streamflow in Southern Québec

by

Maedeh KHALILI

THESIS PRESENTED TO ÉCOLE DE TECHNOLOGIE SUPÉRIEURE
IN PARTIAL FULFILLEMENT FOR THE MASTER'S DEGREE
WITH THESIS IN CONSTRUCTION ENGINEERING
M.A.Sc.

MONTREAL, JUL 20TH, 2026

ÉCOLE DE TECHNOLOGIE SUPÉRIEURE
UNIVERSITÉ DU QUÉBEC

**BOARD OF EXAMINERS**

THIS THESIS HAS BEEN EVALUATED

BY THE FOLLOWING BOARD OF EXAMINERS

Mrs. Annie Poulin, Thesis Supervisor
Département du génie de la construction, École de technologie supérieure

Michel Baraër, Member of the jury
Department of construction engineering, École de technologie supérieure

Mr. Richard Arsenault, President of the jury
Department of construction engineering, École de technologie supérieure

THIS THESIS WAS PRENSENTED AND DEFENDED

IN THE PRESENCE OF A BOARD OF EXAMINERS AND PUBLIC

JUN 5$^{TH}$, 2026

AT ÉCOLE DE TECHNOLOGIE SUPÉRIEURE

# ACKNOWLEDGMENT

I would like to express my sincere gratitude to my supervisor, Dr. Annie Poulin, for her continuous support, guidance, and valuable feedback throughout this work. Her expertise and encouragement were essential to completing this study. I truly valued every moment of this experience, learned so much, and am truly grateful for it all.

I would like to acknowledge the support of Philippe Lucas-Picher, Professor of Atmospheric Sciences at UQAM, who made it possible for me to work in the Linux environment at UQAM. This opportunity greatly facilitated my research process.

I'm dedicating a special thanks to my husband, Zakaria, for his unwavering encouragement, patience, and support. His belief in me and constant motivation played an invaluable role in achieving this milestone.

My family members in Iran, who always support me with their love and encouragement. I am so grateful for your support throughout every stage of this journey, though miles away.

I would also like to thank all my friends and lab colleagues, Siavash, Mina, Mariana, Behmard, Freya, Melike, and Hadis, for their understanding, encouragement, and support throughout the project.

**Comparaison de simulations climatiques régionales avec une résolution de convection et une résolution plus grossière pour l'évaluation des précipitations et du débit des cours d'eau dans le sud du Québec**

Maedeh, KHALILI

## RÉSUMÉ

Comprendre comment la résolution des modèles climatiques influence la représentation des événements hydrométéorologiques intenses est crucial pour améliorer l'évaluation des risques d'inondation. La plupart des études sur les impacts du changement climatique ont utilisé des simulations de modèles régionaux climatiques (MRC) avec des résolutions spatiales supérieures à 10 km. La paramétrisation de la convection profonde est nécessaire pour simuler les événements convectifs avec les MRC, qui reflètent les effets moyens de la convection. Ceci peut introduire une incertitude et conduire à une sous-estimation des précipitations extrêmes. Des travaux récents ont démontré que les modèles climatiques à haute résolution (avec résolution spatiale de 1 à 4 km) permettent d'améliorer les simulations des précipitations extrêmes infra-journalières par rapport aux modèles climatiques régionaux à plus faible résolution.

Dans cette étude, nous utilisons trois simulations horaires du modèle WRF (Weather Research and Forecasting) (ci-après nommées CONUS, CORDEX 22 et CORDEX 44), toutes alimentées par la réanalyse ERA-Interim, à différentes résolutions spatiales de 4 km, 25 km et 50 km. Notre objectif est de comparer les profils de précipitations et de températures dans des simulations couvrant trois saisons (avril-mai, été et automne) à une résolution temporelle horaire sur le sud du Québec, au Canada. L'analyse des précipitations a permis de constater que le modèle WRF avec une résolution de 4 km (simulation CONUS) a produit les valeurs RX1-heure (précipitations maximales sur 1 heure) les plus élevées durant l'été. En revanche, les deux simulations CORDEX présentent des profils de précipitations comparativement moins intenses.

Nous avons ensuite analysé l'impact de ces différences sur la modélisation hydrologique. Pour ce faire, nous avons simulé le débit des cours d'eau à l'aide d'un modèle hydrologique global (GR5dt) à un pas de temps horaire, sur douze bassins versants du sud du Québec (superficies de 61 à 1 550 km²). Nous avons utilisé les données de précipitations issues du produit de précipitations dérivées de satellites (IMERG) et les données de température ERA5-Land comme jeux de données de référence pour calibrer le modèle hydrologique. Les résultats montrent qu'en avril-mai, les températures plus élevées de la simulation CONUS entraînent une fonte des neiges plus précoce et un débit plus faible. À l'inverse, les deux simulations CORDEX avec des températures plus froides ont accumulé davantage de neige, ce qui a entraîné des crues de fonte plus tardives et plus importantes.

Concernant le biais sur les débits de pointe annuels, l'analyse des données CONUS a généralement montré que ces débits de pointe sous-estimés, en particulier durant l'été, malgré des intensités de précipitations horaires plus élevées. Cela peut être expliqué par les températures plus élevées de la simulation CONUS qui tendent à augmenter l’évapotranspiration potentielle simulée. Cependant, une étude de cas sur un petit bassin versant indique que la simulation CONUS est en mesure de produire des événements hydrométéorologiques intenses et de courte durée qu’on ne retrouve pas avec les simulations CORDEX22 et CORDEX44.

**Mots-clés** : simulations climatiques WRF, simulation à haute résolution permettant la convection (CONUS), précipitations extrêmes, débit de pointe

**Comparison of convection-permitting and coarser-resolution regional climate simulations for evaluating precipitation and streamflow in Southern Québec**

Maedeh, KHALILI

## ABSTRACT

Understanding how climate model resolution affects the representation of heavy and intense hydrometeorological events is crucial for enhancing flood risk assessment. Most studies on the impacts of climate change have utilized Regional Climate Model (RCM) simulations with spatial resolutions coarser than 10 km. Deep convection parameterization is necessary to simulate convective events with RCMs, which reflect the averaged effects of convection. This may thus introduce uncertainty and can lead to underestimation of extreme rainfall. Recent work has demonstrated that high-resolution climate models (with grid spacing of 1-4 km) have the capability to improve simulations of sub-daily extreme precipitation compared with coarser-resolution regional climate models.

In this work, we use three simulations of hourly Weather Research and Forecasting (WRF) model configuration (hereafter called CONUS, CORDEX 22 and CORDEX 44), all driven by the ERA-Interim reanalysis, at different spatial resolutions of 4 km, 25 km, and 50 km. We aim to compare precipitation and temperature patterns across simulations for three seasons (April-May, Summer, and Fall) at hourly temporal resolution over southern Québec, Canada. In terms of extreme precipitation analysis, we found that the WRF model with 4-km (CONUS simulation) produced the highest RX1-hour values (Maximum 1-hour Precipitation) during the summer. In contrast, the two CORDEX simulations show precipitation patterns that are comparably less intense.

We further analysed how these differences extend into hydrological modelling. To do so, we simulated streamflow using a lumped hydrological model (GR5dt) at hourly time steps, across twelve southern Quebec watersheds (surface areas of 61–1550 km²). We used Satellite-derived precipitation product (IMERG) precipitation data and ERA5-Land temperature as our reference datasets for calibrating the hydrological model. The results show that during April-May, the higher temperatures from the CONUS simulation lead to earlier snowmelt and lower streamflow. Conversely, the two CORDEX simulations with colder temperatures accumulated larger snowpacks, resulting in delayed and more noticeable spring floods.

The analysis of CONUS generally showed that simulated annual peak flows were underestimated, particularly during the summer, despite the model representing higher hourly precipitation intensities. This can be explained by the higher values of simulated potential evapotranspiration due to CONUS higher temperatures. However, a case study of a small watershed indicates that the CONUS simulation is capable of generating intense, short-duration hydrometeorological events that are not observed in the CORDEX22 and CORDEX44 simulations.

**Keywords**: WRF climate simulations, high resolution convection permitting (CONUS) simulation, extreme precipitation, peak flow

# TABLE OF CONTENTS

Page

## LIST OF TABLES

**LIST OF FIGURES**

**LIST OF ABREVIATIONS**

| | |
|---|---|
| CONUS | Contiguous United States |
| CPM | Convection-Permitting Model |
| ECCC | Environment and Climate Change Canada |
| ECMWF | European Centre for Medium-Range Weather Forecast |
| ERA-Interim | European Retrospective Analysis Interim |
| ERA5-Land | ECMWF Reanalysis 5th Generation - Land |
| GCMs | General Circulation Climate Models |
| GR5-dt | A lumped conceptual rainfall-runoff model |
| HYDROTEL | A semi-distributed and physically-based hydrological model |
| IMERG | Integrated Multi-satellitE Retrievals for GPM |
| IPCC | Intergovernmental Panel on Climate Change |
| JJA | June July August |
| KGE | Kling Gupta Efficiency |
| LBC | Lateral Boundary Conditions |
| MCS | Mesoscale Convective Systems |
| NA-CORDEX | The North-American Coordinated Regional Downscaling Experiment |
| PET | Potential Evapotranspiration |
| RCMs | Regional Climate Models |
| RX1-hour | Max 1-hour precipitation amount |
| SON | September October November |
| SWE | Snow Water Equivalent |
| WRF | Weather Research and Forecasting |

# INTRODUCTION

Heavy precipitation events have grown more frequent and intense across North America as a result of human-caused climate change. These events and associated flood risks are projected to increase due to this ongoing warming (IPCC 2022)

While recent studies have focused considerable attention on this topic, previous work has primarily utilized coarse-resolution GCMs (grid spacing > 100 km), which have deficiencies in capturing extreme precipitation events and in underestimating their frequency (Wang, Zhang, and He 2017; Li et al. 2012). These GCMs typically generate significant biases when simulating extreme precipitation, often producing overestimations for low-intensity precipitation (i.e., drizzle) while underestimating high-intensity events (Piani et al. 2010).

Regional climate models (RCMs) were therefore developed around 1989 to address the computational limitations (Boville and Gent 1998). The models have become a valuable tool for higher-resolution climate change projections (Tapiador et al. 2020). In fact, their use of a limited-area domain, fed at its boundaries by global datasets (e.g. from reanalyses or GCMs), allows computational resources to be concentrated regionally, representing finer spatial detail than is typically possible with GCMs (Lucas-Picher et al. 2024). A large body of research has employed RCM output to force hydrological models to reproduce river discharge and flood behavior (Kay, Jones, and Reynard 2006; Teutschbein and Seibert 2010; Li et al. 2017).

While these models offer several advantages, conventional RCMs with grid resolutions of 10 km or more still depend on parameterized deep convection, and this introduces substantial modeling uncertainty (Prein et al. 2015; Fosser et al. 2020). In addition, even with the use of bias-corrected GCM outputs to force RCMs at resolutions coarser than 10 km, the inheritance of GCM biases by RCMs remains a major challenge (Kim et al. 2020; Xie, Li, Chen, Mayer, et al. 2025).

Given that parameterized convection cannot accurately simulate local extreme events, convection-permitting regional climate models (CPMs) with grid resolutions finer than 4 km were introduced. These high-resolution models emerged about a decade ago and represent a significant advancement in regional climate modeling. They constitute a major improvement in the ability to resolve convective systems and provide deeper insight into the impacts of climate change (Dallan et al. 2024). This is because they explicitly resolve convective processes and avoid the constraints imposed by deep convection parameterization. CPMs' ability to resolve deep convection and localized extremes enables a more realistic simulation of daily and sub-daily precipitation characteristics parameterization (Prein et al. 2015; Berthou et al. 2020). This includes improvements in representing the diurnal cycle, the intensity and frequency of heavy rainfall, spatial and temporal patterns, and the duration of wet and dry spells (Xie, Li, Chen, Mayer, et al. 2025; Dallan et al. 2023). The ability of CPMs to simulate hourly and daily precipitation extremes, including their return periods, frequencies, and intensities, has been underlined particularly in Europe (Alpine areas) (Dallan et al. 2023; Giordani et al. 2023).

Despite overall improvements in precipitation simulations, the extent to which these improvements propagate to hydrological modeling and simulated floods at basin scales is yet to be determined. Some studies have used CPMs and indicate that the models can successfully reproduce observed river discharge behavior across various regions. For instance, Poncet et al. (2024) used the convection-permitting CNRM-AROME CPM (2.5 km) and its driving CNRM-ALADIN RCM (12 km) to assess extreme rainfall and flood responses in a Mediterranean watershed. According to their results, 2.5 km simulations reproduced extreme rainfall and flood peaks more realistically than their driving RCM. In southern Quebec, Sabzipour et al. (2025) studied climate outputs from the CRCM6/GEM5 model at 2.5 km resolution and from its coarser 12 km version. Their results showed that the 2.5 km model simulation represented extreme hourly rainfall intensities more accurately than the 12 km simulation, when compared with station-based observations.

They also indicated these improvements extended to the reduced biases in flood peaks compared with the 12 km simulations.

However, some research has shown that CPMs did not improve flood simulations, even though they improved precipitation representation. For instance, in a historical evaluation study in western Norway, Xie, Li, Chen, Mayer, et al. (2025) used a convection-permitting model (CPM) and its coarser-resolution reanalysis-driven counterpart (HCLIM) as hydrological forcing and compared it against observed precipitation, temperature, and discharge to assess whether the convection-permitting model improves flood simulation. They discovered that a 3-km CPM produced more realistic high-intensity rainfall; nevertheless, it did not show clear added value for flood simulations compared with the coarser 12 km model. Reszler, Switanek, and Truhetz (2018) examined CPMs across small to medium-sized (ranging from 30-1000 $km^2$) Alpine catchments and found that although higher-resolution models improved heavy-precipitation representation, this did not consistently lead to better flood peak simulation. Kay et al. (2015) demonstrated that simulated discharge did not improve because the model showed a wet bias during heavy precipitation across the UK.

The conclusions derived from these comparisons are inconsistent across the literature. Hydrological studies based on CPM simulations are therefore required for more comprehensive evaluations of this new generation of climate models across different climates and basins.

In southern Québec, Canada, floods are typically linked to spring snowmelt or to intense rainfall during the summer and fall seasons. As the climate continues to warm across southern Québec, snowmelt-driven floods are anticipated to reduce, whereas rainfall-induced floods are likely to increase in both frequency and intensity (Brissette et al. 2023). Over the last two years, southern Québec has experienced two extreme flooding events, underscoring the significant impacts of extreme precipitation. The most recent one, which occurred in August 2024, southern Québec ('Weather events 2024') experienced intense rainfall due to the remnants of Hurricane Debby. Some regions, such as the Laurentians and Lanaudière, experienced over 150 mm of rain within 24 hours, resulting in flooding during August 9 to 10. With an estimated insured loss of around CAD 2.5 billion, this incident is the most expensive weather disaster in the province's history ('Weather events 2024'). Southern Québec and the St. Lawrence Valley experienced another heavy storm in July 2023 during the convective season. Localized rainfall totals reached 50 to 90 mm, with some stations reporting 85 mm in just two hours ('Weather events 2023').

The region’s vulnerability to short-duration extreme rainfall is highlighted by these events, especially in small, fast-responding watersheds. The present study aims to evaluate the impact of increased spatial resolution on systematic differences in climate simulations using WRF model simulations at different resolutions. Hence, we used three ERA-Interim-driven climate simulations from the Weather Research and Forecasting (WRF) model at different spatial resolutions to assess whether higher spatial resolution results in systematic differences in climate simulation outcomes. Thus, this setup enables us to assess the effects of different spatial resolutions based on the following hypotheses: (1) Given that all three datasets are all from the WRF model with the same reanalysis boundary forcing, significant differences in simulated spring-freshet precipitation are not expected. (2) The CPM WRF simulation will generate heavier summer-fall precipitation and associated flooding than the other coarser WRF simulations, especially in small-scale watersheds.

# CHAPITRE 1

# LITERATURE REVIEW

This chapter focuses on presenting the key topics that are fundamental to understanding and contextualizing the methods used to conduct this study. The topics covered, in order of appearance, are: climate models, hydrological modeling, hydrological modelling classification and uncertainty.

## 1.1 Climate Models

The term General Circulation Model or global climate models (GCM) refers to a numerical model that simulates the global climate by computing the hourly evolution of the three-dimensional atmosphere, based on the conservation of mass, momentum, energy, and water vapor (Grotch and MacCracken 1991). The dynamical core and the physical model are the two main components of all climate models, referred to as global climate models (GCMs). The dynamical core uses classical equations to simulate large-scale atmospheric and oceanic motions, whereas the physical model simulates key climate-related processes such as radiation, cloud microphysics, and convection. These interactions usually occur on scales smaller than the numerical grid of the models, making it challenging to capture them accurately. The models incorporate the impacts of aerosols, heat exchanges between the ocean and atmosphere, and friction between land or ocean surfaces and the air, among many other processes (Palmer 2019). To account for these small-scale processes on a larger scale, instead of simulating them, modelers use "parameters," for instance, mathematical functions and constants. The most crucial aspect of climate modeling, which has sparked considerable scientific and political debate, is the precise parameterization of these physical processes (Berner et al. 2017). GCMs usually operate at a formal grid spacing of between 100 and 200 kilometers. Their real resolution, however, is much coarser, on the order of 6–8 grid cells, closer to ~1000 km. This deficiency prevents them from capturing regional and local processes such as intense precipitation (Rummukainen 2010). Historically, enhancing resolution to the kilometer scale in GCMs has been too costly and computationally intensive

(Schär et al. 2020). It is then well demonstrated that even moderate increases in the spatial resolution of Global Climate Models (GCMs) can enhance the simulation of small-scale extreme precipitation events in mid-latitude regions (Wille et al. 2025; Wehner et al. 2014). However, merely enhancing model resolution without adjusting other model parameters is insufficient to improve the accuracy of extreme precipitation representation significantly (Bador et al. 2020).

Regional climate models (RCMs) were therefore generated to downscale the coarse climate fields produced by global climate models (GCMs). This progress delivered higher-resolution information suitable for regional climate analyses and for vulnerability, impacts, and adaptation (VIA) assessments (Giorgi 2019). Two main downscaling approaches are commonly used: statistical and dynamical. In terms of statistical downscaling, the links between local variables like temperature or precipitation and large-scale climate patterns such as mean sea level pressure are created. Dynamical downscaling, in contrast, uses regional climate models (RCMs) that follow the same physical and dynamical laws as global climate models (GCMs) (Vogel et al. 2023). RCMs offer added value over GCMs by incorporating finer-scale information about regional features (Giorgi 2019). The near-surface wind patterns in complex coastal regions are more accurately represented by RCMs. They also improve the simulation of mesoscale variations in surface pressure and temperature. Also, RCMs successfully replicate the typical features of moderate daily precipitation across a few grid cells (Ha et al. 2024). An increase in resolution further improves the model's ability to represent synoptic and mesoscale phenomena, including frontal systems, precipitation processes, and extreme weather events (Rummukainen 2010). Given that convection occurs at scales of a few kilometers, parameterization is required in conventional RCM simulations with grid resolutions between 10 and 100 km (Fosser, Khodayar, and Berg 2015). However, one major source of uncertainty in representing precipitation characteristics arises from the parameterization of convection (Brockhaus, Luthi, and Schar 2008).

As computational capacities were enhanced, RCMs spatial resolutions reached to grid resolutions < 4 km, at which deep convective processes can be directly represented in the model instead of through parameterization which have been previously identified as a source of model uncertainty (Fosser, Khodayar, and Berg 2015; Lucas-Picher, Argüeso, et al. 2021). Thus, convection-permitting regional climate models (CPMs) are essentially RCMs scaled up to explicitly simulate deep convection (Prein et al. 2015; Lucas-Picher, Argüeso, et al. 2021). The finer resolution of CPRMs also allows for better representation of landscape features such as coastlines, mountains, and urban areas (Kendon et al. 2021; Lucas-Picher, Argüeso, et al. 2021).

By explicitly resolving convective systems and improving the representation of local-scale processes, CPRMs produce a more accurate simulation of sub-daily precipitation as the primary motivation for using CPRMs (Kendon et al. 2017). This includes improved representation of the diurnal cycle, spatial precipitation structure, intensity distributions, and extreme events (Prein et al. 2015; Fosser, Khodayar, and Berg 2015). Thereby, CPRMs with deep convection accurately simulated, have shown added values compared to conventional RCMs that parameterise convective processes (Lucas-Picher, Argüeso, et al. 2021). Improved simulation of short-duration precipitation extremes over complex terrain (orographically complex regions) (Dallan et al. 2023), better representation of 2-m temperature in western Canada (Li, Li, and Li 2020), better representation of small scale wind systems (Belušić et al. 2018), tropical cyclones (Gentry and Lackmann 2010), land-atmospheric interactions (Taylor et al. 2013), and monsoons (Marsham et al. 2013) are added values in CPM-based models that have been shown over several domains. Furthermore, CPMs better represent local-scale climate conditions given their higher spatial resolution, which allows them to characterize surface heterogeneities in greater detail. As a result, more accurate simulations of regional meteorological events are produced (Lucas-Picher, Laprise, and Winger 2017). In terms of extreme precipitation, improved representation of hourly precipitation, the diurnal cycle and the frequency of extreme precipitation events have been shown in previous studies (Prein et al. 2015; Fosser, Khodayar, and Berg 2015). Overall, CPRMs better simulate short-duration precipitation extremes compared to coarser-resolution models(Kendon et al. 2017; Fosser et al. 2024).

CPM forcing offers advancements for hydrological applications as well. It provides additional dynamical downscaling of variables that require high spatial and temporal resolution while preserving the physical consistency between variables (Lucas-Picher, Argüeso, et al. 2021). A growing number of studies have employed CPMs in hydrological applications to investigate future flood risks. While some studies showed higher performance in simulating flooding events using CPMs (Lee, Bae, and Im 2019; Qing et al. 2020), others did not reach a clear advantage of these models (Reszler, Switanek, and Truhetz 2018).

Multi-year convection-permitting climate simulations are computationally demanding due to higher model resolution, which significantly increases computing costs (approximately 10 times). As a result, studies are often limited in terms of simulation length, ensemble size, or area-domain extent. This may affect the reliability of the uncertainty assessments and extreme-event statistics (Kendon et al. 2021), though it enables the production of convection-permitting climate projections at a computationally feasible cost (Giorgi 2019). Although advances in supercomputing power are making CPM simulations more affordable (Leutwyler et al. 2017), running multi-year global simulations at convection-permitting resolution remains challenging. This can suggest regional kilometre-scale models will continue to be required for affordable climate projections (Kendon et al. 2021).

Regarding general rules, CPMs adopt the same nesting techniques as RCMs, since CPMs are essentially an extension of RCMs (Giorgi 2019). However, due to their higher resolution, CPMs require more frequent updates of the lateral boundary conditions, typically every hour, compared to the six-hour intervals used for conventional RCMs (Fosser et al. 2020). The resolution ratio of 12 represents the maximum recommended difference between the coarse driving model and the nested regional model. The approach originally adapted for RCMs continues to be applied to CPMs (Berthou et al. 2020). This ensures that the large-scale process provided by the driving model remains consistent at finer resolutions. Traditional multi-nesting techniques, also known as telescopic nesting (downscaling is run in several steps), utilize RCMs as intermediate step to derive kilometer-scale CPMs from coarse-resolution GCMs (>100 km) (Lucas-Picher, Argüeso, et al. 2021). This approach allows for adherence to the maximum value step of 12 (Denis, Laprise, and Caya 2003). Recent research, however, has evaluated the performance of higher-resolution simulations when the intermediate nesting step is removed. The studies indicate that the direct nesting approach can be beneficial mainly because it allows significant savings in time and computational resources (Raffa et al. 2021). The improved performance of simulating intense precipitation has also been demonstrated by direct-nesting ensembles (Marsigli, Montani, and Paccagnella 2014).

## 1.2 Flooding Sensitivity to Extreme Precipitation

Small watersheds are particularly sensitive to convective precipitation events because their spatial scale is comparable to that of individual thunderstorm cells (Sharma, Wasko, and Lettenmaier 2018; Reszler, Switanek, and Truhetz 2018). Consequently, a convective storm is likely to impact most of a small watershed's area. It saturates soil moisture rapidly and increases the fraction of rainfall that becomes rapid runoff, ultimately producing more severe flooding. It has been found that smaller watersheds (usually less than 1000 $km^2$) tend to undergo increases in flood magnitude, whereas larger basins are more prone to decreases in peak flows. (Do, Westra, and Leonard 2017; Llasat et al. 2016; Lemaitre-Basset et al. 2021). As relatively new tools in this area, CPMs have been used only in a limited number of hydrological modeling studies. Consequently, their benefits for hydrological processes remain uncertain. For example, Zhang, Wang, and Wang (2021) reported an intensification of flood risk across several basins in southern Texas, USA. According to Kay et al. (2015), a 1.5 km CPM did not improve river flow simulations compared to a 12 km RCM in 32 catchments. They also underlined the sensitivity of small catchments to intense summer rainfall and the complexity of modeling these systems. Another study that used two CPMs, Kay and Brown (2023), found that fast-responding catchments generally show improved performance, whereas some catchments show degradation.

In northern areas such as Quebec, Canada, flooding events can occur due to two main factors. The first is a combination of spring runoff resulting from an extreme snowpack, along with simultaneous rainfall and melting conditions. The second is caused by summer or fall runoff events that can result from a significant rainstorm (Rousseau et al. 2014). As the climate warms in southern Quebec, according to the research by Brissette et al. (2023) it is expected that springtime snowmelt floods will gradually decrease, while the frequency and severity of summer and fall floods will increase. These summer and fall floods are solely due to extreme rainfall, and they tend to reach relatively higher peaks in small to medium-sized watersheds (those less than 500 $km^2$), particularly when the size of the watershed is comparable to the meteorological system causing the rainfall.

## 1.3 Hydrological Modeling

A hydrological model represents real-world hydrological systems in a simplified framework. The model can be described as a set of equations that allow for the estimation of discharge based on several parameters used to describe the characteristics of a watershed (Devia, Ganasri, and Dwarakish 2015). These models are primarily used to predict system behavior and understand various hydrological processes (Moradkhani and Sorooshian 2009). The two essential types of input data for all models are meteorological data, including precipitation and temperature, along with watershed characteristics, such as watershed area, soil properties, vegetation cover, topography, soil moisture content, and groundwater characteristics. Hydrological models are constructed using mathematical formulas and statistical assumptions. The models can be vulnerable to many climatic and physiographic variables, according to Meresa et al. (2023).

### 1.3.1 Classification of hydrological models

Rainfall–runoff models are characterized by their required inputs and their parameters, as well as by the extent to which physical principles are represented (Devia, Ganasri, and Dwarakish 2015). Over the last few decades, researchers have classified hydrological models by complexity, accessibility, input/output type, user-friendliness, temporal resolution, and level of spatial aggregation. Hydrological models are commonly classified into three spatial categories: fully distributed, semi-distributed, and lumped (Meresa et al. 2023). They can also be categorized based on their representation of physical processes, distinguishing between conceptual and physically based models.

Spatially distributed hydrological models offer spatially detailed representations of the natural heterogeneity inside the modeled watershed's domains (Euser et al. 2015). The models produce spatially distributed outputs by dividing the entire catchment area into small units, typically a two-dimensional grid or a triangulated irregular network, so that parameters, inputs, and outputs can vary spatially. Distributed runoff models represent the highest level of complexity because they consider spatial heterogeneity in model inputs and parameters (Sitterson et al. 2018). Distributed models are data-intensive, as all input variables are represented in both space and time. Each grid cell has a distinct hydrological response that is computed individually while accounting for interactions with neighboring cells (Rinsema 2014). By providing spatially explicit hydrological information, distributed models have played an important role in management applications, including agricultural and ecological impact studies. See e.g., (Rode et al. 2010; Bouadi et al. 2017).

Semi-distributed models are extensions of lumped models that incorporate certain characteristics of distributed models, allowing partial representation of spatial variability within a watershed. In these models, the watershed is divided into smaller units, each with distinct parameter values. Sub-basins can be divided by slope, soil group, vegetation zone, or into smaller units known as hillslopes, within which hydrological processes are assumed to be uniform and homogeneous, similar to lumped models (Esteves 1996). hillslopes are typically defined by overlaying maps of land cover, soil type, and elevation. The flow generated within each HRU or sub-basin is subsequently routed and attenuated to the watershed outlet (Beven 2012).

Lumped models provide a representation of the entire model domain without spatial discretization. They capture the impact of small-scale natural heterogeneities through simple flux parameterizations that apply to the larger scale of the model domain. Lumped models can be applied to systems at various scales, ranging from soil samples to river basin scale, as long as the resulting functional relationships accurately capture the effects of heterogeneity within the domain (Hrachowitz and Clark 2017b). According to Beven (2012) the models are simple to use and require little computer power, but they are most effective when streamflow at the catchment outlet is the only factor to consider. The information provided by these models is not spatially distributed. Popular lumped models include HBV (Bergström 1995) and GR4J (Perrin, Michel, and Andréassian 2003).

Physically based models aim to provide a detailed understanding of the hydrological system by describing the processes that control the flow of water, energy, and solutes in the soil, and between the land, vegetation, and atmosphere (Hrachowitz and Clark 2017a). These models are intended to depict the complex interactions occurring at various scales and are based on the physical laws and principles that control the system. The models attempt to explicitly represent as many processes as possible, including infiltration, evapotranspiration, and groundwater flow, to provide a mechanistic description of the hydrological system. This allows for a more accurate representation of the system and can offer insights into the effects of changes in factors like land use, climate, and other factors on the hydrological cycle (Hrachowitz and Clark 2017a). The ideal circumstance is when every component of a model, such as boundary conditions and system states, is completely understood. It is also possible to build functional relationships between states and fluxes in these circumstances, which are known as closure relations or flux parameterizations. These relations directly emerge from observations and principles of mass, momentum and energy conservation without further assumptions or calibration. However, since most observations are available only at small scales, physically based models may be used to describe the system at the microscale (Hrachowitz and Clark 2017a). The distinction here is important. Single observations offer lumped characterizations of a flow system that combines spatial heterogeneities and variety in processes that are smaller in scale than the observation itself. To be valid, physically based models operate in a lumped manner at the observation scale because additional discretization under the observation scale would require further assumptions about the heterogeneity of grid cells. Besides, physically based models need to explicitly account for landscape details to be effective. Therefore, they must be distributed spatially at larger scales, allowing for the transformation of the information from observations over space (Grayson and Blöschl 2001).

Conceptual models offer a macroscale explanation of the hydrological system and more condensed, abstract representations of the underlying processes. In this context, the term "macroscale" refers to any scale larger than that of a single microscale observation used in physical models. Although the complexity of internal system processes is usually neglected, expanding to the macroscale integrates inherent microscale variations and their interactions across the entire model domain (Fenicia et al. 2016). Conceptual models use relatively simple flux parameterizations to describe the hydrological system at a large scale based on the integrated observations available at that scale (e.g. streamflow). These models are intended to represent the large-scale effects of small-scale heterogeneities that emerge at the scale of the model application. Unlike physically based models, conceptual models represent fewer individual hydrological and thermodynamic processes. For instance, instead of detailed representations of land-atmosphere energy fluxes, they use the empirical concept of potential evaporation to describe evaporative processes (Hrachowitz and Clark 2017a; Fenicia et al. 2016). Since numerous system boundary conditions and states of the hydrological system can not be directly measured at the macroscale, the way that conceptual models describe the movement of water through the system (through flux parameterizations) can have many uncertainties. Therefore, assumptions must be made about the shape of these flux relationships, or their parameters may need to be calibrated to match observations (Kumar, Samaniego, and Attinger 2010). One advantage of conceptualizing hydrological systems is that it allows for the concentration of key processes on a large scale rather than attempting to model every little aspect. This approach reduces the number of required model parameters, but it does not necessarily lead to a loss of information. Instead, it allows for the integration of heterogeneous processes at the microscale. It provides a system description consistent with observed data at the scale of interest without the need for further assumptions and the corresponding uncertainties (Zehe et al. 2014). The use of traditional lumped conceptual models without adequate testing and evaluation may lead to oversimplifications and overlook the effects of natural heterogeneity on hydrological responses. Nevertheless, conceptual models can be constructed to incorporate varying levels of process and spatial complexity, depending on the availability and quality of relevant information (Gharari et al. 2011). The fact is all models involve some degree of conceptualization (Haghnegahdar et al. 2015).

### 1.3.2 Uncertainty

Climate change impact assessments involve several methodological choices, including selecting climate models, greenhouse gas emission scenarios, bias-correction methods, and hydrological models. Since different choices may deliver different future outcomes, it is essential to explore a range of approaches to evaluate their effects and quantify associated uncertainties (Bastola, Murphy, and Sweeney 2011; Ludwig et al. 2009). The uncertainty cascade is classified into the different components of the hydroclimatic modeling chain, with the principal elements relevant to this study described below. Climate models typically represent natural processes using physical equations and parameterizations. A limited understanding of underlying processes requires the use of various simplifications and parameterization schemes, and this can lead to different outputs for the same input data (Kundzewicz et al. 2018). The use of RCMs and other downscaling techniques adds an additional source of uncertainty to regional climate projections. In general, downscaled regional climate projections are influenced by multiple uncertainties that propagate through each stage of the modeling process (Giorgi 2005).

The main sources of uncertainty include emission scenarios, GCM responses to a given emission scenario, internal variability, and the choice of RCM or various downscaling methods (Giorgi 2019). Some research has shown that climate model uncertainty is the main source of uncertainty compared to other sources such as downscaling methods and hydrological models (Joseph et al. 2018; Chen et al. 2011). However, uncertainty assessment remains challenging in convection-permitting simulations due to the use of a single model or/and single simulation, and this limitation is amplified at finer scales where local processes increase internal variability (Coppola et al. 2020). Due to computational constraints, convection-permitting ensembles can be limited in spatial extent and can hardly be able to fully represent uncertainty. Statistical methods, including new machine learning approaches, combined dynamical-statistical approaches and process-informed bias correction are being developed to bridge this gap by integrating coarse-resolution multi-model outputs with limited CPM simulations (Kendon et al. 2021; Coppola et al. 2020). However, research on this matter has started to grow. Fosser et al. (2024) found that the CPM ensemble can decrease overall uncertainty by up to 50%. Besides, they concluded that even more reliable local projections can be expected by improved representation of local processes in CPMs, which is critical for adaptation planning. In a recent study, Bian et al. (2026) used 15 WRF model simulations at a 3 km grid scale. They evaluated how different parameterization schemes can affect precipitation characteristics relevant to hydrological applications. They showed that using optimized convection-permitting models allows for the representation of precipitation features and provides useful guidance for hydrological modeling across complex terrain.

Hydrological model uncertainties are driven by parameter values, model structure, calibration data, and input variables. It can also result from additional uncertainties associated with model initial and boundary conditions.

Hydrological models often include parameterizations derived from conceptual simplifications, commonly referred to as effective parameters (Moges et al. 2021). Parameter uncertainty stems from the challenges in estimating effective parameters that represent conceptualized hydrological processes, as well as from natural variability and observation errors. Although some parameters can be measured at the point scale, their variability at the catchment scale is difficult to capture.

Even with a perfect model structure, errors in calibration data can introduce additional uncertainty, often leading to a lack of a unique optimal parameter set (Beven 2006). The uncertainty arising from model structure is commonly known as structural uncertainty (Krysanova et al. 2018). All modeling choices, including process representation, numerical methods, spatial and temporal resolutions, and the representation of topography, soil, and vegetation contribute to structural uncertainty (Krysanova et al. 2018). Ensemble-model techniques, which combine different model structures, allow for an effective way to quantify and assess structural uncertainty (Moges et al. 2021; Beven 2012; Thiboult, Anctil, and Boucher 2016).

## CHAPITRE 2

## COMPARISON OF CONVECTION-PERMITTING AND COARSER-RESOLUTION REGIONAL CLIMATE SIMULATIONS FOR EVALUATING PRECIPITATION AND STREAMFLOW IN SOUTHERN QUÉBEC

Maedeh Khalili[1], Annie Poulin[1], Siavash Pouryousefi Markhali[1]

[1] Department of Construction Engineering, École de technologie supérieure, 1100 Notre-Dame West, Montreal, Quebec, Canada H3C 1K3

Paper submitted to Journal of Hydrology: Regional Studies, May 2026

### 2.1 Abstract

**Study Region:**

Southern Quebec, Canada

**Study Focus:**

This study evaluates seasonal precipitation and temperature (April-May, summer, fall), as well as Rx1-hour (maximum hourly) precipitation across study area domain, using 3 climate simulations, all configured by Weather Research and Forecasting (WRF) regional climate model, driven by ERA-Interim reanalysis, at spatial resolutions of 4 km (CONUS simulation), 25 km, and 50 km (two CORDEX simulations). The simulations were further fed into a conceptual hydrological model to simulate streamflow at an hourly time step across twelve southern Quebec watersheds with surface areas ranging from 61–1550 km². Satellite-derived precipitation product (IMERG) precipitation and ERA5-Land temperature serve as our reference datasets for hydrological model calibration.

**New Hydrological Insights for the Region:**

The 4 km simulation (CONUS) produced the highest summer Rx1-hour precipitation values. In April-May, CONUS simulation produces lower mean snow water equivalent (SWE) than those of the CORDEX simulations, primarily due to higher temperatures, which lead to earlier snowmelt and lower mean streamflow peaks compared to CORDEX simulations. Although CONUS simulation produces higher extreme summer

precipitation, this does not necessarily translate into higher streamflow simulations, most likely because higher temperatures tend to increase potential evapotranspiration. However, event-based analysis in a small watershed showed CONUS simulation is able to produce short-duration, high-intensity rainfall events that do translate streamflow peaks that are not found in the CORDEX simulations.

**Keywords**: WRF climate simulations, high resolution convection permitting (CONUS) simulation, extreme precipitation, peak flow

## 2.2 Introduction

Floods are occurring more frequently and more intensely across the globe, which is mainly caused by more intense rainfall events (Xie, Li, Chen, Mayer, et al. 2025; Tabari 2020). Although hydrological impact studies have traditionally relied on corrected outputs from global climate models (GCMs) (Vogel et al. 2023), their coarse spatial resolution (Vogel et al. 2023) and inherent biases (Di Luca, Pitman, and de Elía 2020) cause limits in their ability to accurately simulate precipitation extremes occurring at the fine spatial scales required for impact modeling. Nevertheless, GCMs remain effective in representing large-scale climate processes  (Rummukainen 2010).

Regional climate models (RCMs) were developed to downscale coarse-resolution GCM outputs and have advanced substantially over the past decades (Giorgi 2019). Improvements in spatial resolution from ~25 to 50 km to higher scales finer than 10 km (Rummukainen 2010) have enhanced the representation of spatial detail and extreme climate events (Christensen and Christensen 2007; Rummukainen 2010). RCMs have been widely employed in climate and hydrological impact studies, including the simulation of precipitation extremes and river discharge (Mailhot et al. 2007; García-García et al. 2020; Nazarian et al. 2022; Lucas-Picher, Lachance-Cloutier, et al. 2021). However, they tend to underestimate precipitation extremes (Goergen and Kollet 2021), largely due to limitations in convection parameterization, which is critical for representing short-duration, high-intensity events such as those, for instance, leading to summer flash floods (Fosser et al. 2024).

Computational advances in refining RCMs' grid resolution (< 4 km) allowed for explicit simulation of deep convection instead of parameterizations, a common practice in the past resulting in a significant source of modeling uncertainty (Lucas-Picher, Argüeso, et al. 2021; Kendon et al. 2012). The growing use of convection-permitting models (CPMs) in climate research arises from their enhanced ability to simulate hourly precipitation (Prein et al. 2015). Several recent studies have used convection-permitting models and demonstrated their strong skill in reproducing hourly precipitation, including the diurnal cycle, the spatial distribution of precipitation, intensity distribution, and extreme events (Vanden Broucke et al. 2019; Fosser et al. 2024; Wille et al. 2025; Liu et al. 2017). For example, Fosser et al. (2024) used CPM ensemble simulations to examine future changes in hourly precipitation and projected increases in extreme events. Wille et al. (2025) compared simulations against satellite-based products, reanalysis, and gridded observations across hourly and daily scales. Vanden Broucke et al. (2019) using daily observations and limited hourly station measurements have also shown that simulated hourly precipitation extremes align with observations.

Unlike all these advantages for enhancement in the representation of sub-daily and extreme precipitation, there are some studies that have also highlighted remaining limitations. For example, Dallan et al. (2023), using hourly precipitation from rain gauges, showed that although a 2.2 km CPM reproduced the overall patterns of extreme rainfall in the Italian Alps, it tended to overestimate hourly extremes.

A recent study by Xie, Li, Chen, Mayer, et al. (2025) compared two regional climate simulations against gridded and situ observational datasets over Norway. They applied the HCLIM3, 3 km CPM versus HCLIM12, 12 km RCM. Based on their results, in terms of hourly extremes and at local scales, HCLIM3 consistently outperformed HCLIM12, except with no benefits at the regional scale. Akinsanola et al. (2024) carried out a multi-decadal climate simulation at 4 km resolution throughout North America. Incorporating a number of gridded observations, their results showed a better representation of this simulation regarding seasonal and extreme precipitation when compared to ERA5, however they still reported regionally large errors. Using a group of sub-daily gridded precipitation datasets (based on weather stations and radar estimates), Lucas-Picher et al. (2024) showed that a 2.5 km CNRM simulation improves the representation of sub-daily precipitation extremes relative to its 12 km driver. However, they reported that both models still exhibit persistent dry and wet biases in seasonal mean precipitation and temperature. So, representing daily and sub-daily extremes remains challenging particularly in regions with complex terrain (Dallan et al. 2023). The ability of CPMs to improve simulations of extreme precipitation at local and basin scales remains an ongoing area of research.

Despite the fact that CPMs are potentially promising tools, they have only been used in a limited number of hydrological impact studies, though the body of research in this field is beginning to expand. A few studies have explored the added value of CPMs for flood simulations. For instance, Poncet et al. (2024) used the CNRM-AROME CPM (2.5 km) and its driving CNRM-ALADIN RCM (12 km) against an observed precipitation gridded product to assess extreme rainfall and flood simulations in a Mediterranean watershed. According to their results, 2.5 km simulations reproduced extreme rainfall and flood peaks more realistically than their driving RCM**.** In a recent study across southern Québec, Sabzipour et al. (2025) compared the outputs of the CRCM6/GEM5 model at 2.5 km resolution with those of its coarser 12 km version. They found that the 2.5 km CPM more accurately simulated extreme hourly precipitation events compared with hourly weather station data. They found that those improvements translated into reduced biases in flood peaks compared with the 12 km simulation.

Other studies have not yet demonstrated constant improvements in simulated discharge and flood modeling using CPMs. For example, according to Reszler, Switanek, and Truhetz (2018) CPMs did not show a clear enhancement in flood simulation performance across Europe. Based on the recent study by Xie, Li, Chen, and Xu (2025), CPMs improve the representation of extreme precipitation and temperature. However, such improvements do not always surpass RCMs in flood simulation performance.

Despite the growing body of literature evaluating the influence of regional climate model spatial resolution on climate and hydrological impact simulations, there remains a limited understanding of the extent to which increased spatial resolution consistently improves the simulation of precipitation extremes and their hydrological responses.

Southern Québec is particularly relevant because flooding commonly results from spring snowmelt or from summer and fall extreme precipitation events. Continued warming is expected to reduce snowmelt-driven floods, while at the same time, rainfall-induced floods are projected to increase in both frequency and intensity (Brissette et al. 2023). In recent years, the region has faced significant hydrological impacts such as widespread flooding because of heavy rainfall from Hurricane Debby's remnants in August ('Weather events 2024') and severe convective storms in July 2023 ('Weather events 2023'). These events highlight the region's vulnerability to short-duration heavy rainfall, particularly in small, fast-responding watersheds. To address this knowledge gap, the present study uses three ERA-Interim-driven Weather Research Forecast (WRF) historical climate simulations at three different spatial resolutions, 50, 25 and 4 km. The simulations are evaluated for seasonal precipitation and temperature during April–May, summer, and fall, as well as hourly precipitation extremes (Rx1-hour), and are used to drive a conceptual hydrological model for twelve southern Québec watersheds. This experimental design enables assessment of the effect of climate model spatial resolution while minimizing the effects of differences in model configurations. We study the effects of different spatial resolutions based on the two following hypotheses:

(1) since all three simulations originate from the same (WRF) regional climate model driven by ERA-Interim reanalysis, substantial differences in simulated spring-freshet are not expected;
(2) the CPM (4km) simulation will generate more intense summer-fall precipitation and associated flood simulations than the other two (50 and 25 km) WRF simulations, particularly in small-scale watersheds.

## 2.3 Study area and data

### 2.3.1 Study area

This study focuses on twelve snow-dominated watersheds in southern Quebec, Canada, with sizes spanning from 61 km² to 1550 km² according to Table 2.1. The primary factor for the selection process was the availability of hourly hydrometeorological data. Figure 2.1 shows the watersheds used in the study area. Three watershed size categories were established: small, medium and large. We used colored contours to distinguish different sizes: black for small (<300 km2), green for medium (>300 km2 and <700 km2), and blue for large (>700 km2) watersheds. This enables us to assess whether climate forcing differences impact hydrological responses across various scales.

Table 2.1 General characteristics of each watershed used in this study

| Size | Names | IDs | Watershed area (km2) | Mean annual precipitation (mm/year) | Mean annual temperature (C°) |
|---|---|---|---|---|---|
| Small | Boyer Sud | 023002 | 61 | 1178.21 | 4.91 |
| | Morpions | 030423 | 94.1 | 1182.84 | 6.92 |
| | Bras d'Henri | 023432 | 154 | 1212.64 | 5.14 |
| Medium | Des Hurons | 030415 | 308 | 1134.47 | 6.89 |
| | L'Acadie | 030421 | 367 | 1112.58 | 7.15 |
| | Du Loup | 022507 | 515 | 1103.14 | 3.67 |
| | Eaton | 030234 | 646 | 1248.79 | 4.73 |
| | Brasdu Nord | 050409 | 646 | 1207.75 | 2.44 |
| Large | Au Saumon | 030282 | 769 | 1233.21 | 4.22 |
| | Becancour | 024003 | 914 | 1214.91 | 4.73 |
| | Etchemin | 023303 | 1152 | 1167.81 | 4 |
| | Nicolet | 030103 | 1550 | 1196.04 | 5.56 |

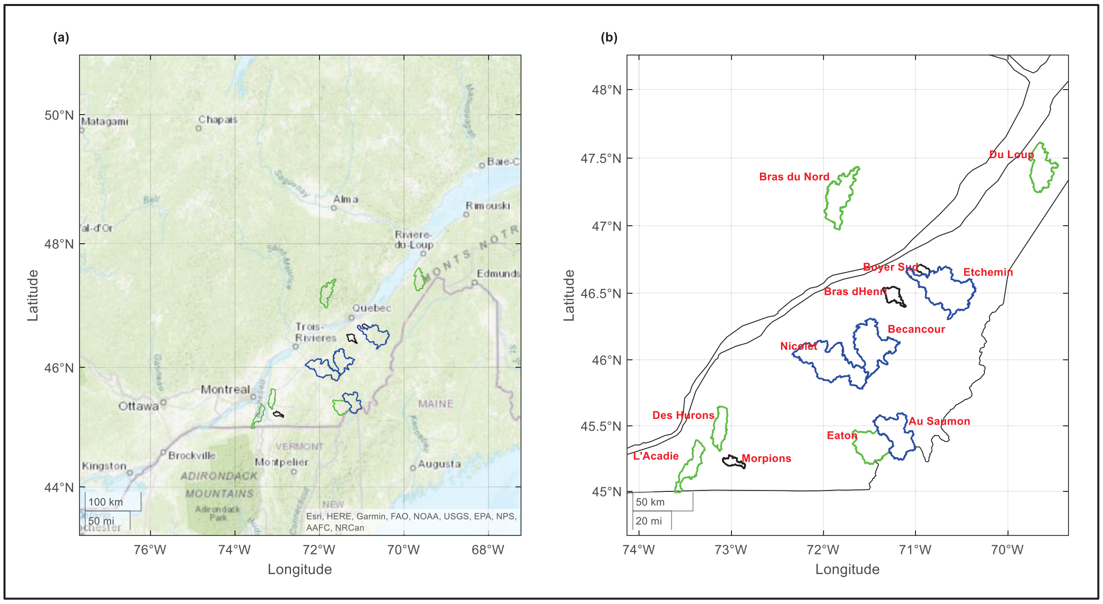


Figure 2.1 Locations of watersheds across southern Quebec. Black, green, and blue colours correspond to small (<300 km2), medium (>300 km2 and <700 km2) and large (>700 km2) watersheds respectively, a) the larger extent, b) the smaller extent

### 2.3.2 Hydrometeorological Data

Hourly precipitation, temperature, and discharge data, were sourced from multiple datasets, including ERA5-Land, IMERG and three WRF climate simulations hereafter called CONUS (at 4km) and NA-CORDEX (at 25 and 50 km) as well as the 3 nearest weather stations. Observed streamflow data were obtained from the Ministère de l'Environnement, de la Lutte contre les Changements Climatiques, de la Faune et des Parcs (MELCCFP 2025). We gathered the data over the 2001-2020 time period in hourly time steps.

ERA5-Land is a high-resolution global reanalysis dataset produced by the European Centre for Medium-Range Weather Forecasts (ECMWF) for the Copernicus Climate Change Service (C3S). It provides hourly data at 0.1° spatial resolution (~9 km), with a detailed representation of land surface conditions from 1951 to the present. ERA5-Land is created by running ECMWF's land surface model, using downscaled ERA5 atmospheric forcing, including corrections for elevation effects. The dataset consistently represents the evolution of the water and energy cycles over land, which makes it suitable for analyzing trends, anomalies, and hydrological processes (Muñoz-Sabater et al. 2021). ERA5-Land shows improved performance in representing soil moisture, lake conditions, and river discharge over ERA5 and ERA-Interim reanalyses (Muñoz-Sabater et al. 2021). Linear interpolation was used to obtain ERA5-Land-driven precipitation, which downscales the spatial resolution from approximately 31 km in ERA5 to about 9 km in ERA5-Land. The temporal resolution remains at the hourly scale, similar to ERA5 (Wu et al. 2023).

Integrated Multi-Satellite Retrievals for GPM (IMERG) Version 06 (V06) is a satellite-based precipitation product that merges and calibrates data from various sources, including passive microwave and infrared sensors aboard satellites, as well as ground-based observations. Most data originate from the Global Precipitation Measurement Mission (GPM) constellation, particularly its core satellite equipped with the Dual-polarization Radar and GPM Microwave Imager. IMERG V06 is accessible at 0.1° resolution and 30-minute intervals (Bélair et al. 2024)**.** IMERG has generally been used for a variety of applications due to its comparatively high spatial (0.1°) and temporal (30 minutes) resolutions (Sun et al. 2018) and good representation of precipitation distribution (Chen et al. 2021; Su et al. 2019). Table 2.2 presents a summary of the hydrometeorological datasets used in this study.

Table 2.2 Overview of the hydrometeorological datasets utilized in this study

| Dataset | Spatial resolution | Temporal resolution | Variable(s) | Data coverage |
|---|---|---|---|---|
| Discharge Stations (MELCCFP) | - | 1 hour | River discharge | 1997-2022 |
| Reanalysis ERA5-Land (ECMWF) | ~9 km | 1 hour | Temperature | 1950- 2023 |
| Observation-Satellite IMERG/ Version 06 (V06) | ~ 10 km | 30 minutes | Precipitation | 2000-2021 |

### 2.3.3 Climate simulations

The 4-km CONUS (CONUS 1) simulation was run using the Weather Research and Forecasting (WRF) Model version 3.4.1 covering a large portion of the continental United States (CONUS), southern Canada and northern Mexico. Its Boundary conditions were provided by the ERA-Interim reanalysis dataset (0.7° resolution, 6-hourly) (Liu et al. 2017). The CONUS simulation allows the explicit representation of convection and improves the resolution of mountainous terrain. It spans from October 1, 2000, to September 30, 2013 (Rasmussen and Liu 2017).

The NA-CORDEX simulations using WRF model version 3.5.1 include outputs over a domain encompassing most of the continental United States (Rendfrey et al. 2021). The time period of the NA-CORDEX simulations cover from 1980 to 2010 (McGinnis and Mearns 2021).
The common time period to all three simulations is 2001–2010 and will therefore be considered for the remainder of this study, which focuses on the northern region of the simulations' domains (approximately 42°N to 49°N) in southern Québec. The domain coverage is shown in Figure 2.1. In the remaining figures of the paper, we refer to high-resolution CONUS simulations as C1, and the CORDEX simulations at resolutions of 0.22 and 0.44 as C22 and C44, respectively. Table 2.3 summarizes the relevant information, with respect to the present study, for each of the three simulations. More complete information about the WRF simulations can be found in Liu et al. (2017) and in Rendfrey et al. (2021).

Table 2.3 Information about the three climate simulations

| Climate simulations | CONUS simulation | NA-CORDEX simulations |
|---|---|---|
| Regional climate model | WRF model Version 3.4.1 | WRF model version 3.5.1 |
| Spatio-temporal resolution | 4 km, hourly | 0.22°/25km, hourly<br>0.44°/50km, hourly |
| Driving global dataset | Global driving dataset: ERA-Interim<br>Time span: October 2000-September 2013 | Global driving dataset: ERA-Interim<br>Time span: 1980-2010 |
| Deep convection | explicit | parameterized |
| Reference papers | (Liu et al. 2017) | (Rendfrey et al. 2021) |

## 2.4 Methodology

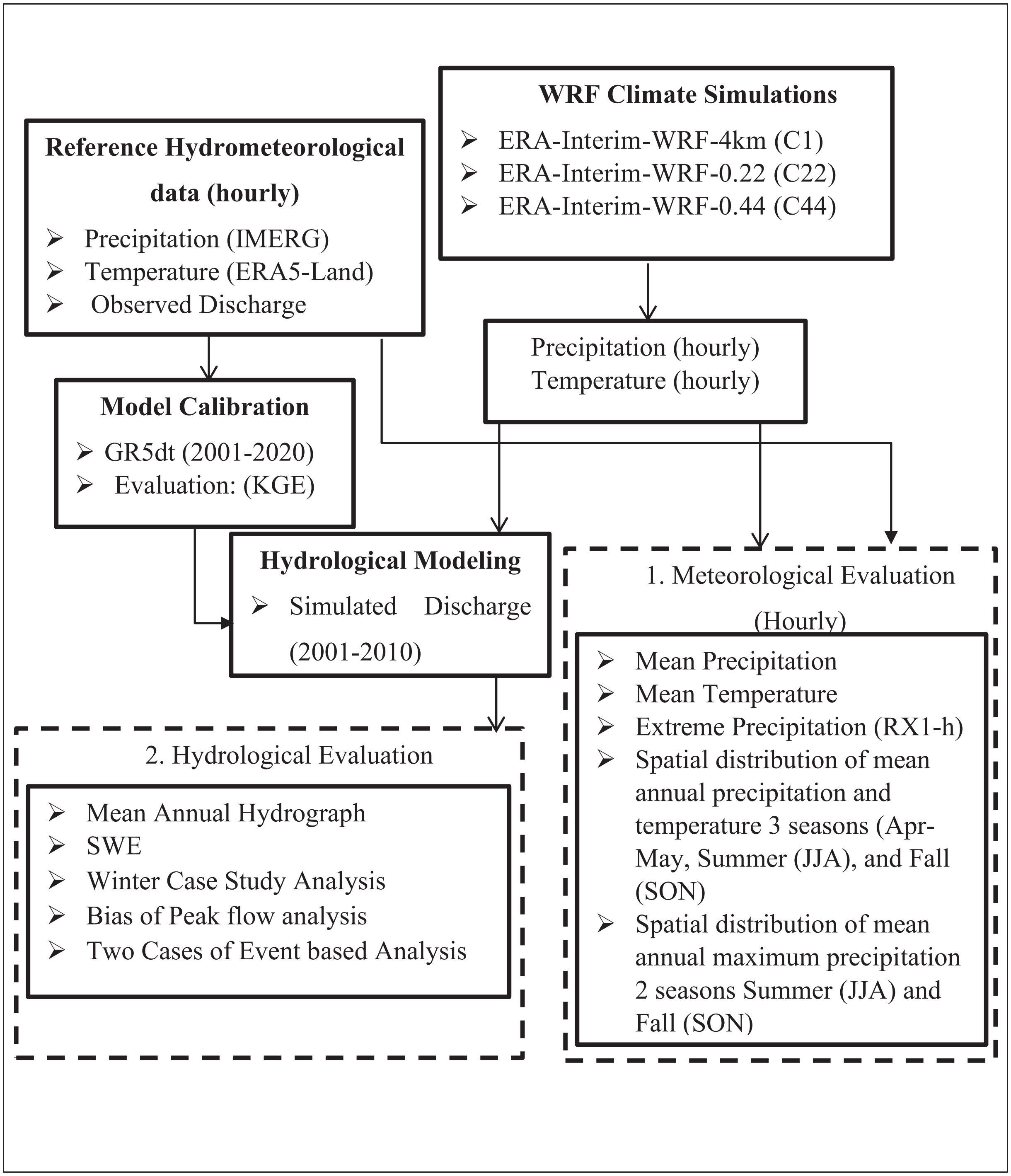


Figure 2.2 The methodological framework used in this study

Figure 2.2 presents the complete overview of the methodological framework used in this study. The dashed lines correspond to the specified metrics used to analyze the two research hypotheses of this paper.

### 2.4.1 Meteorological evaluation

We extracted hourly precipitation and temperature data for 12 selected watersheds in southern Quebec from the IMERG and ERA5-Land reference datasets as well as from the three climate simulations as shown in figure 2.2. As the hydrological model that was used is lumped (see section 2.4.2), areal averaged precipitations and temperature time series had to be generated. At least four grid points inside or surrounding (when necessary) the watersheds' boundaries were weighted using Thiessen polygons for those with an area less than 100 km². The corresponding weights were then applied to the corresponding grid points to generate the areally-averaged time series. We used a standard mean for averaging the data from all grid points inside the watersheds' boundaries for the watershed with sizes larger than 100 km². The closest weather stations are used to compare with selected grid points from IMERG and ERA5-Land in terms of extreme precipitation. Only three stations were used for this comparison, due to the limited availability of hourly station data during the matching period (2005-2019). This analysis allows us to choose between ERA5-Land and IMERG. However, the comparison is not presented here, IMERG performed better than ERA5-Land in representing extreme precipitation (RX1-hour). As a result, hourly precipitation data from IMERG were selected as the reference dataset for hydrological model calibration.

The evaluation metrics to test our hypotheses regarding meteorological evaluations consist of (Figure 2.2): the spatial distribution of mean total precipitation, mean temperature, and maximum 1-hour precipitation (RX1-hour). As shown in Figure 2.2, mean total hourly precipitation and mean hourly temperature were calculated for three periods: April–May (Apr–May), summer (June, July, August - JJA), and fall (September, October, November - SON). The maximum hourly precipitation was then computed for each summer and fall season. All these computations were done from 2001 to 2010 at each grid cell. After computing the seasons' RX1-hour values for each year, we computed the mean value across the 10 years of available data. The mean

RX1-hour values were used to assess seasonal extreme rainfall events across the simulations. It is given as follows:

$$Mean\ RX1hour\ = \frac{1}{N}\sum_{j=1}^{N} max_i\ (RRij) \quad (2.1)$$

$RRi$ = precipitation at hour i (in mm/hour), $j$ = a defined period (e.g., a season or a year), $max_i$ $(RRij)$ = the seasonal maximum hourly precipitation values in that period (for the year $j$). $N$ = the number of years. $RX1hour$ = the seasonal maximum hourly precipitation for the year $j$.

### 2.4.2 Hydrological modelling and evaluation

River discharge was simulated at an hourly time step using the five-parameters GR5dt lumped hydrological model. GR5dt is a rainfall-runoff model developed for sub-daily time-step simulations (Ficchì, Perrin, and Andréassian 2019), which integrates the lumped GR4J and GR4H models (Perrin, Michel, and Andréassian 2003), using five parameters for calibration. The model consists of two reservoirs: a production store and a routing store. Also, the model is combined with the CemaNeige snow module (Valéry 2010), and the Oudin potential evapotranspiration formulation (Oudin et al. 2005; Oudin, Michel, and Anctil 2005). Here, we briefly explain the snow module. CemaNeige is a degree-day snowmelt module designed to simulate the sub-daily evolution of snow cover. The model enhances river runoff simulations in snow-dominated watersheds by representing snow accumulation, which is defined as the fraction of solid precipitation that accumulates based on air temperature, and the snowmelt, which contributes as liquid precipitation (Riboust et al. 2019). In the accumulation phase, snow cover is assumed to grow linearly with SWE, controlled by temperature-defined thresholds, while the melt process is proportional to the temperature above 0º C. The Cemaneige snow module has two calibration parameters (weighting coefficient and degree-day factor). The combination of GR4J, Oudin and Cemenaige has been extensively used in Canadian catchments and showed strong performance (see e.g. (Huet et al. 2016; Aguilar Andrade et al. 2024)).

We calibrated GR5dt for each of the 12 watersheds from April to November, from 2001 to 2020, as reliable model calibration requires a minimum of 10–15 years of streamflow data (Aguilar Andrade et al. 2024). To calibrate the hydrological model, we used IMERGV06 precipitation data and the ERA5-Land 2-meter air temperature data. We used the shuffled complex evolution optimization algorithm (SCE-UA) (Lei, Li, and Hu 2024) as the optimization method for automatic calibration and the Kling-Gupta Efficiency (Gupta et al. 2009) as the objective function. Arsenault et al. (2014) found the global SCE-UA algorithm to be the most efficient calibration method after comparing ten stochastic optimization techniques, particularly for models with reduced complexity and small parameter spaces (Nemri and Kinnard 2020). KGE has been widely used in hydrology modeling (Pechlivanidis et al. 2014; Santos, Thirel, and Perrin 2018) because of its multi-objective framework, which reduces errors related to bias, variability, and correlation, and is expressed as follows:

$$KGE = 1 - \sqrt{(r-1)^2 + (\alpha-1)^2 + (\beta-1)^2} \quad (2.2)$$

Where $r$ is the correlation coefficient between observed and simulated streamflows, $\beta$ represents the bias ratio and $\alpha$ is the variability ratio (Gupta et al. 2009).

Since the observed discharge data used for calibration were either missing or not reliable during the cold months (December–March), we excluded these months from the calibration period. Model validation was not conducted; instead, all available data were utilized for calibration in line with best practices aimed at maximizing the information content of the parameters, as suggested by Arsenault, Brissette, and Martel (2018), Shen, Tolson, and Mai (2022), and Mai (2023).

Following calibration, the model was run using the obtained calibrated parameter set as well as precipitation and temperature inputs from the three climate simulations (CONUS, CORDEX0.22, and CORDEX0.44), resulting in four different streamflow simulations, one per climate driving simulation (C1, C22 and C44) plus the one resulting from calibration (hereafter called reference simulation). Streamflow simulations were conducted for April–November between 2001 and 2010, which is the overlapping period across all three datasets. Three representative watersheds, one for each of the small, medium, and large categories, were selected to present the patterns of simulated discharge- mean annual hydrograph- in this work. Hourly temperature from CORDEX-0.44 was used to run the hydrological model, along with precipitation from both CORDEX simulations (0.22° and 0.44°), to simulate streamflow, as hourly temperature is not available for the CORDEX-0.22 simulation.

The following evaluation measures are used to test our hypotheses with regards to hydrological analyses as seen in Figure 2.2: mean annual hydrograph, mean snow water equivalent (SWE), one case of daily analysis, focusing on accumulated snow/rain, temperature, SWE, and streamflow during November to May, bias of peak flow, and two cases of event-based evaluation. Here we describe the hydrological evaluation metrics in more detail. First, the mean annual hydrograph has been analysed.

To examine the difference between simulations during the spring freshet corresponding to our first hypothesis, we presented the mean simulated snow water equivalent (SWE) in April from the three climate simulations and the reference dataset over the evaluation period. It was computed from the SWE internal variable extracted from each of the hydrological simulations. Then, to analyze different hydrological processes during the winter period (November to May), we conducted a detailed analysis, focusing on accumulated snow/rain, temperature, SWE, and streamflow on a daily basis for the three representative watersheds. Given the similar behavior observed across the watersheds, we present results for a single watershed.

In order to analyse flood events, we identified these events in the three streamflow simulations by extracting annual peak flows, defined as the maximum river discharge for each of three seasons (April–May (AM), summer (JJA), and fall (SON)). For each peak flow value, the bias relative to the observed peak value, normalized by watershed area (in m³/s/km²), is computed to evaluate the ability of the three simulations to reproduce flood events:

$$Bias = \frac{Q_{sim}^{peak} - Q_{obs}^{peak}}{A} \tag{2.3}$$

Where $Q\ peak\ sim$ and $Q\ peak\ obs$ are the simulated and observed peak streamflows ($m^3\ s^{-1}$), and A is the watershed area ($km^2$). Normalizing by area allows for a consistent comparison of peak-flow performance across watersheds of different sizes. Finally, we aggregated the results across watersheds categorized by size: large, medium, and small.

In order to examine the second hypothesis, two heavy hourly rainfall events along with the corresponding streamflow from the higher-resolution CONUS simulation were extracted in a representative small watershed and compared with those of CORDEX-22- and CORDEX-44-driven streamflow simulations for 2 selected storms (We excluded the Reference simulation because the aim here is to compare the hydrological simulations driven by CONUS (C1), CORDEX (C22 and C44) in this event-based analysis). A spatial distribution of rainfall is created to show the localized intensity of the rainfall events on the associated dates.

## 2.5 Results

### 2.5.1 Precipitation and temperature evaluation

Figure 2.3 compares the mean spatial precipitation distributions between the three climate simulations, including the IMERG dataset (as the precipitation reference dataset), across three seasons: April–May, summer, and fall over the 2001-2010, 10-year period. During April–May, CONUS (C1) simulation reaches the highest mean precipitation with the value of 0.26 mm/h compared to the CORDEX (C22 and C44) simulations with 0.16-0.18 mm $h^{-1}$. IMERG precipitation remains generally lower than the three climate simulations (Figure 2.3a). In terms of mean summer precipitation (Figure 2.3b), the pattern is different, where the CONUS (C1) simulation generally produces lower values than those of the other datasets. CORDEX0.22 (C22) and CORDEX0.44 (C44) simulations show higher mean precipitation across the domain, with maximum values reaching up to 0.27 mm $h^{-1}$, which surpasses those from CONUS and IMERG. CONUS simulation shows lower summer means, with maximum values slightly above 0.23 mm $h^{-1}$. The CONUS drier summer biases align with the results of Liu et al. (2017). Again, as in the case of April-May, IMERG shows a lower maximum mean precipitation during the summer than those of other datasets. During fall (September–November), we observe results similar to those in Apr-May, with CONUS reaching a high of 0.26 mm/h (Figure 2.3c). Here, systematic differences appear in simulated precipitation during the spring freshet, which can partially refute the possibility of the first hypothesis. While CORDEX simulations mean precipitation shows higher values than CONUS during summer (June–August), we cannot confirm or reject the second hypothesis, as this analysis does not examine extreme precipitation. In terms of spatial patterns, the three climate simulations display similar patterns across the three seasons, while IMERG generally remains different.

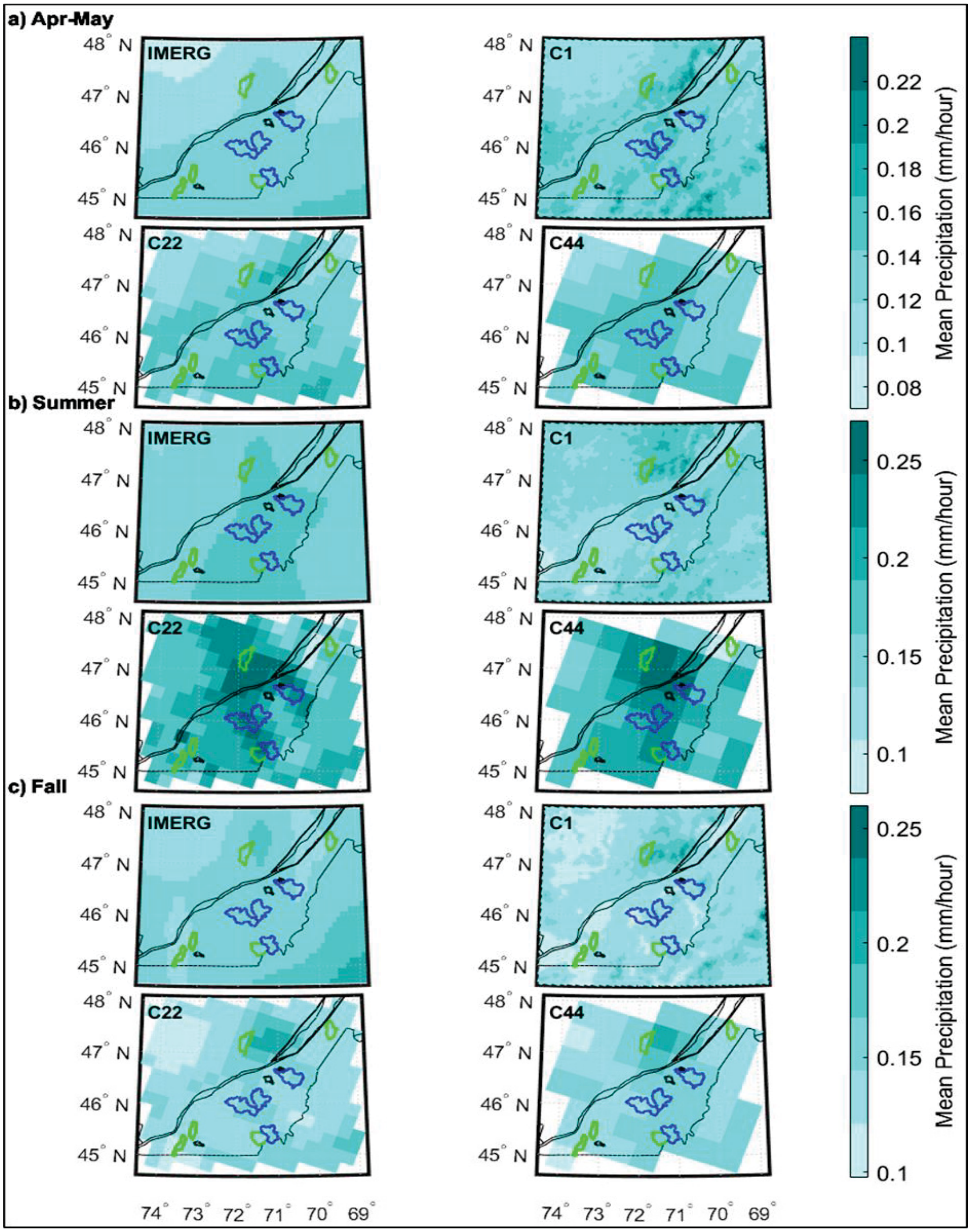


Figure 2.3 Mean seasonal hourly precipitation across the domain for IMERG (reference dataset), CONUS (C1), CORDEX0.22 (C22) and CORDEX0.44 (C44) simulations, (a): spring (April–May), (b): summer (June–August), (c): fall (September–November) over the time period (2001–2010)

Figure 2.4 shows the spatial distribution of mean hourly temperature across the same three seasons as in Figure 2.3. Throughout all seasons (Figures 2.4a, 2.4b and 2.4c), CONUS (C1) simulation consistently shows ~2 °C higher values than CORDEX.44 (C44) and ERA5-Land over the same period. Across all three seasons, we observe that the CONUS simulation shows the widest temperature range, whereas ERA5-Land falls in the moderate category in terms of temperature distribution. CORDEX0.44, having a coarser resolution, displays the narrowest range and the least spatial variability. Particularly, in April-May (Figure 4a), CONUS temperatures reach up to ~12°C in warmer regions, compared to the more limited ranges for ERA5-Land and CORDEX0.44 (~ 2-10°C). During summer (Figure 2.4b), it is noticeable that CONUS generates temperatures ranging from 10°C to 23°C, representing both colder and warmer regions. CORDEX0.44 and ERA5-Land, on the other hand, exhibit more limited temperature variations, remaining within a range of 13–20°C, with their highest mean temperature ~3°C colder than that of CONUS (~23°C). In the fall (Figure 2.4c), the CONUS mean temperature again exhibits the largest spread, extending precisely from 1.5°C to 12.5°C. The warm bias is pronounced in CONUS simulation based on the reference study by Liu et al. (2017). In contrast, this variability is lower in the two other datasets. CORDEX0.44, in particular, underrepresents both the lower and upper temperature means with respect to ERA5-Land (~ 2-8.5°C vs ~ 2-10.5°C). We cannot verify the hypotheses with the results provided here. All three datasets shown on Figure 2.4 show similar spatial patterns, in the three studied seasons.

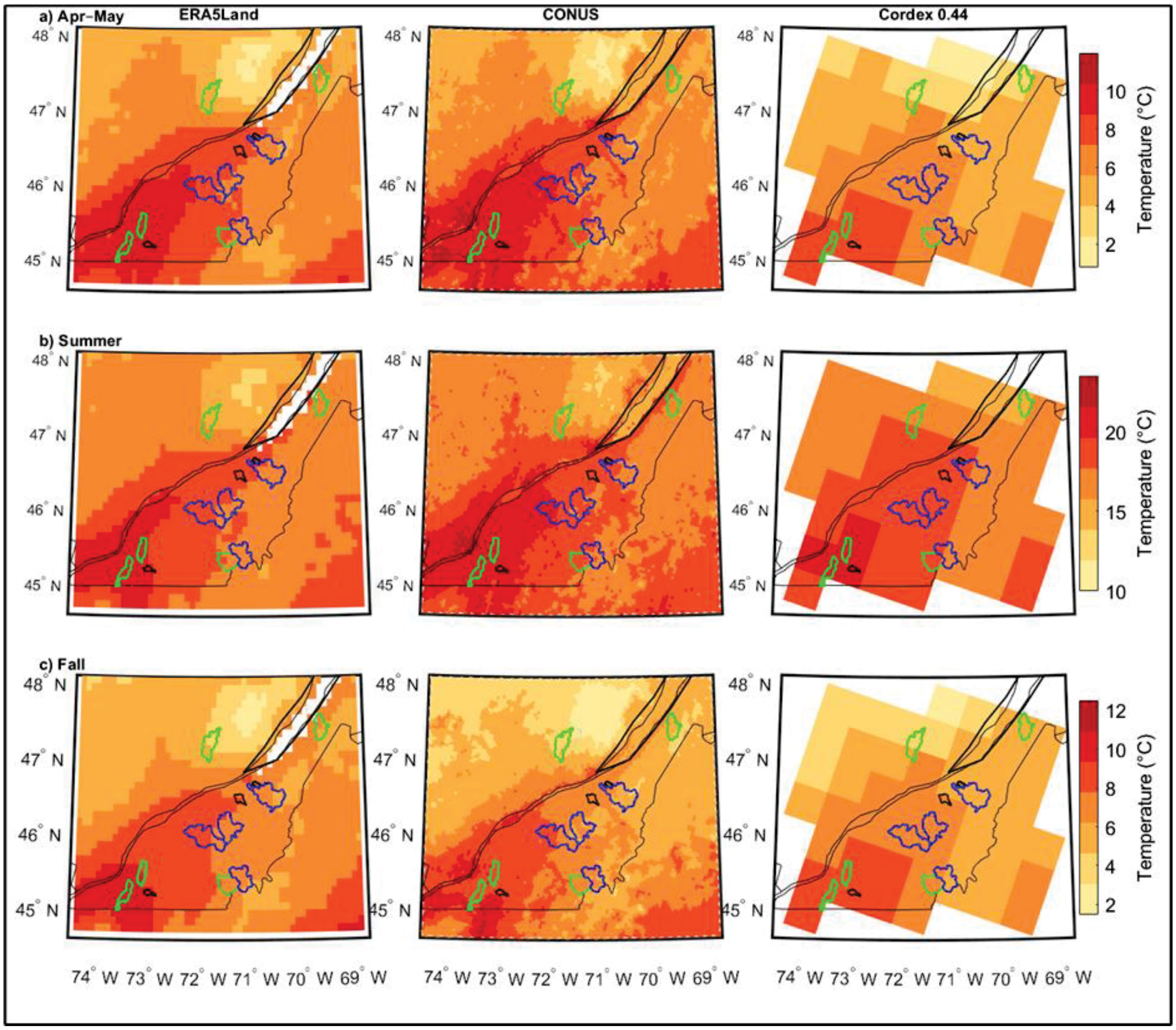


Figure 2.4 Mean Seasonal Hourly Temperature for 3 datasets including ERA5-Land (reference dataset), CONUS (C1) and CORDEX0.44 (C44) simulations, across 3 seasons, (a) spring (April–May), (b) summer (June–August), and (c) fall (September–November) over the time period (2001–2010)

Figure 2.5 presents the spatial distribution of the mean RX1-hour precipitation values for the summer (Figure 2.5a) and fall (Figure 2.5b) seasons across three simulations, CONUS (C1), CORDEX0.22 (C22), CORDEX0.44 (C44), as well as the IMERG reference dataset. In terms of extreme precipitation, we observe the opposite pattern from the previous analysis for mean spatial precipitation (Figure 2.3). Here, during summer (Figure 5a), the CONUS simulation shows the most intense RX1-hour values, which exceed 25 mm/hour in several regions. IMERG and CORDEX0.22 show moderate RX1-hour intensities ranging between ~8 and 18 mm/hour, while CORDEX0.44 generally shows the lowest values with less spatial variability. Therefore, part of the second hypothesis is supported by the extreme precipitation analysis, which can indicate that the CPM (through the CONUS simulation) generates heavier summer precipitation than the other simulations. In the fall (Figure 2.5b), the values decrease consistently across all datasets. IMERG shows the highest peak intensity at 22 mm/h, followed by CONUS with a peak of 19 mm/h. CORDEX simulations produce much lower values, with only a few areas exceeding 14 mm/hour. Their spatial patterns remain smoother, suggesting a limited capacity to capture localized extremes relative to the high-resolution WRF model (and IMERG).

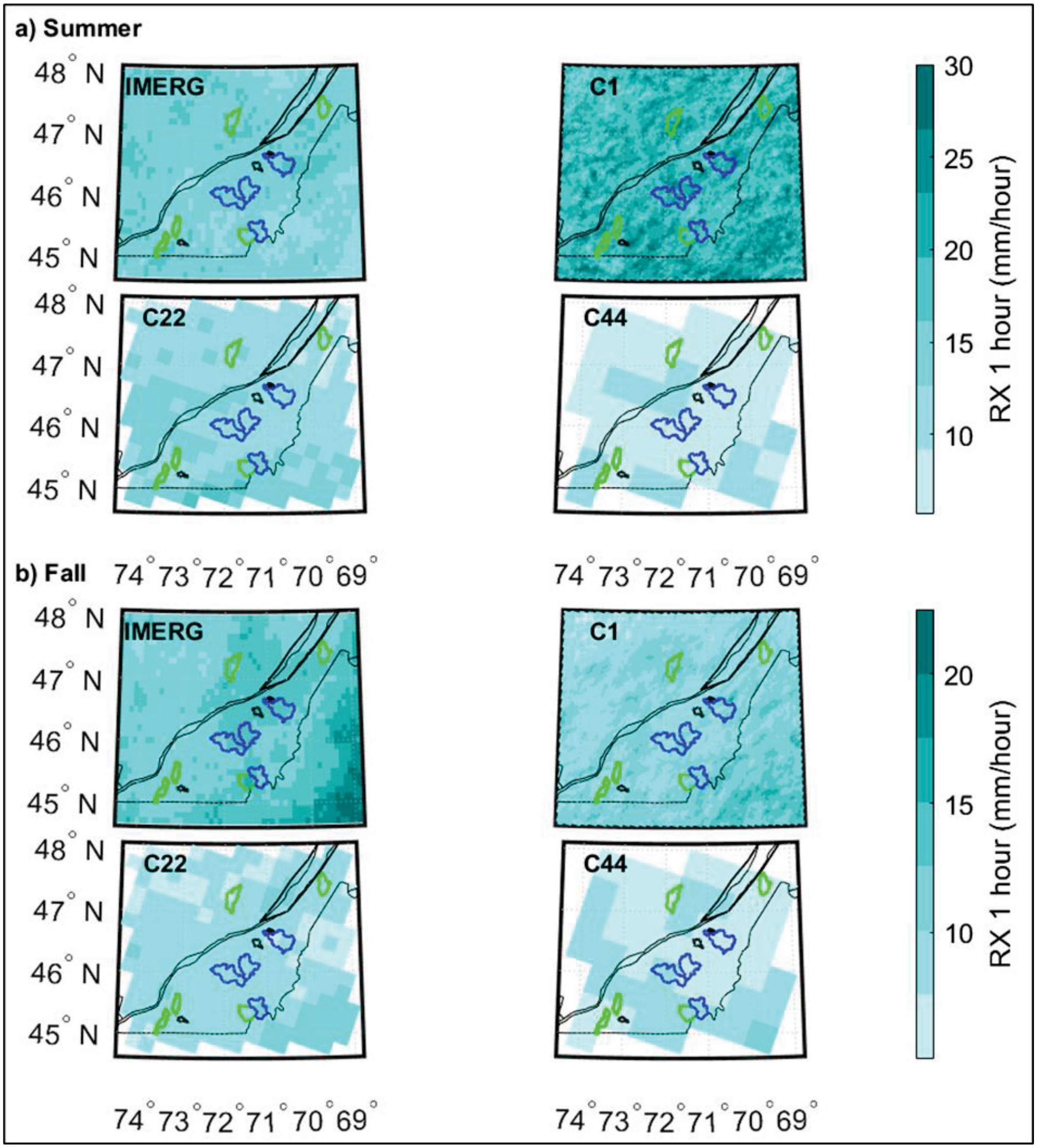


Figure 2.5 Spatial distribution of the mean RX1-hour precipitation for 4 datasets including IMERG (reference dataset), CONUS (C1), CORDEX0.22 (C22) and CORDEX0.44 (C44) simulations, across 2 seasons: (a) summer, (b) fall, over the time period (2001–2010)

### 2.5.2 Hydrological modelling evaluation

#### 2.5.2.1 Calibration performance and mean streamflow hydrograph

Figure 2.6 presents the calibration performance measure (KGE) of the hydrological model (GR5dt) calculated over the calibration period (2001-2020). The watersheds are ordered, in the figure, from left to right, according to growing sizes. All the values are above 0.65, with five out of 12 watersheds having KGE values above 0.8. The lower KGE values in small basins can be due to the fact that they are more susceptible to uncertainties in rainfall input errors and timing, as well as to model structural errors.

Figure 2.7 presents mean annual hydrographs at the outlet of the three representative watersheds: Morpions (small), Du Loup (medium) and Becancour (Large) from April to November. While all watersheds exhibit a dominant spring (Apr-May) freshet, followed by lower summer and fall flows, the degree of variability among the four hydrological simulations differs by both season and watershed scale. The hydrographs (Figure 2.7) show a consistent pattern among datasets. CORDEX0.22 and CORDEX0.44 behave similarly, while CONUS and Reference exhibit similar behaviors. We identified this pattern across all watershed sizes and throughout the April–November period, with the differences being most noticeable in April and May. In large and medium watersheds, all datasets show a clear streamflow peak in April-May, followed by lower summer and fall flows. However, key differences emerge in the timing and magnitude of the Apr-May peak across hydrological simulations, and the contrast is more visible in the medium watershed (Du Loup). In particular, in the large watershed (Becancour), CORDEX0.22 (C22) and CORDEX0.44 (C44) tend to produce higher spring freshet later in early May. CONUS (C1) produces a slightly earlier and lower peak, followed by Reference showing a broader and more gradual rise, in early to mid-April. In the medium size watershed (Du Loup), both timing and magnitude diverge more sharply in Apr-May. CORDEX0.22 and CORDEX0.44 produce similar higher spring freshets in May, while the CONUS-simulated peak is lower and occurs earlier. In contrast, throughout the summer and fall, all datasets indicate slight differences. In the small watershed (Morpions), both CORDEX simulations display that peak streamflow occurs in late April. In contrast, CONUS and Reference indicate an earlier rise in streamflow during early April. This pattern is similar to that observed in two other representative watersheds. Slight differences become visible during summer and fall, where CONUS and Reference tend to produce more frequent and sharper peaks in this small watershed. At the same time, CORDEX-driven simulations show smoother, more subdued simulated discharge. So, the first hypothesis concerning the differences in simulated spring-freshet precipitation among different simulations is not verified based on the results.

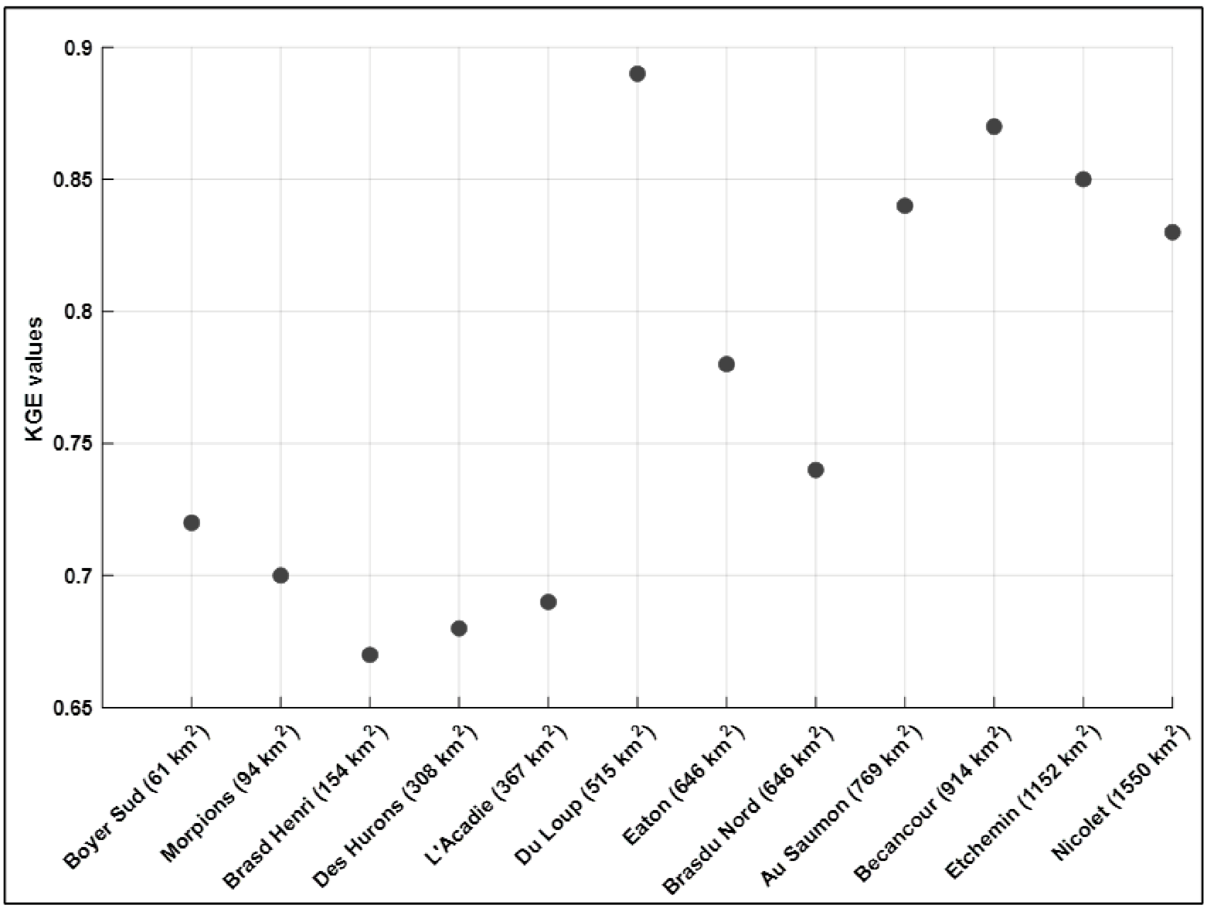


Figure 2.6 Calibration performance for all watersheds (KGE) (2001–2020)

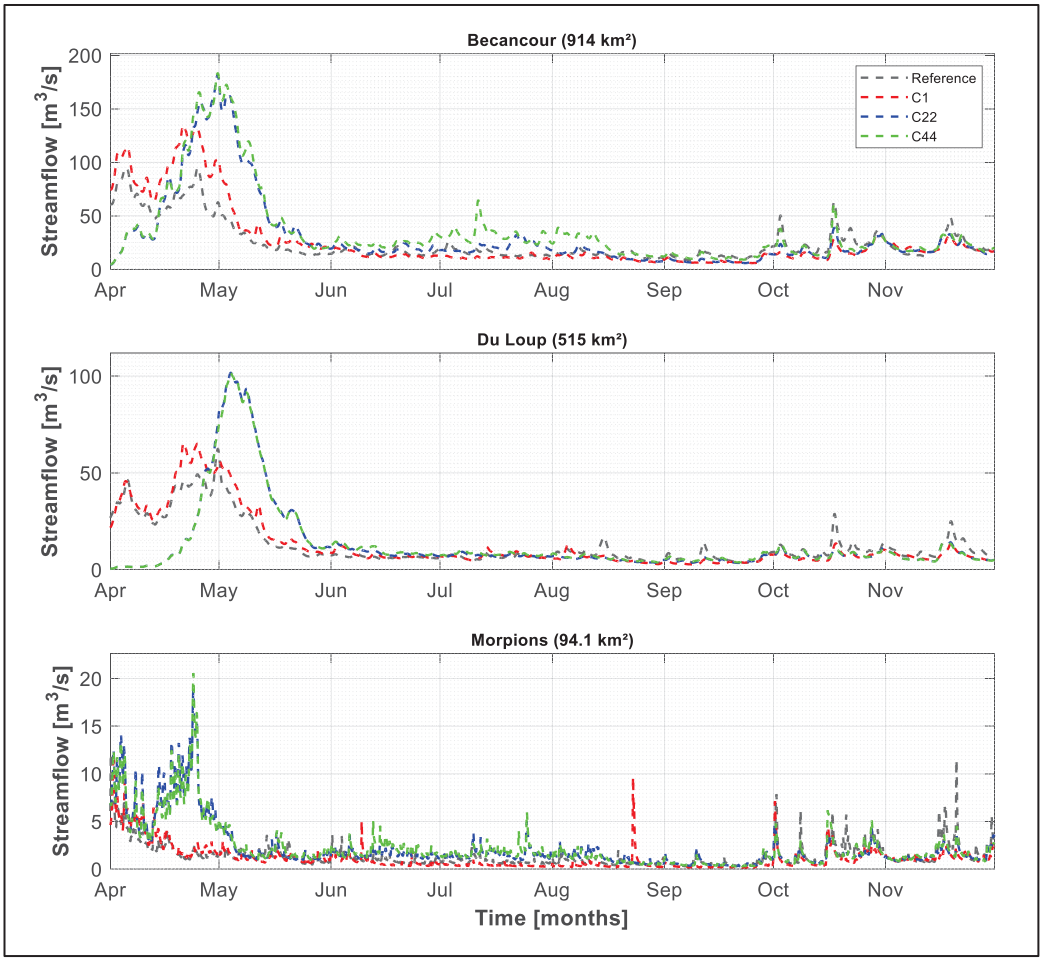


Figure 2.7 Mean annual hydrograph in the representative large (Becancour), medium (Du Loup), and small (Morpions) watersheds

### 2.5.2.2 SWE Analysis

In order to evaluate the April and May discrepancies among the datasets, we quantified the snowpack conditions across all 12 watersheds in April, where we noted significant differences. So, this measure helps for validation of the first hypothesis. We excluded May from this analysis because it could yield zero values in some watersheds, which could have a large impact on the mean values. Figure 2.8 presents the mean snow water equivalent stored in the snowpack. The results show that throughout April, the Reference and CONUS (C1) datasets produce lower values of SWE than those of the two CORDEX (C22 and C44) simulations across all watersheds. In fact, snowmelt begins earlier in both Reference and CONUS-driven simulations, given their higher temperatures, which explains this pattern. In contrast, both CORDEX simulations show higher snow water equivalent (SWE) in April, which indicates a delay in melt onset due to the lower temperatures in CORDEX0.44. These differences in snowpack are consistent across all watersheds (and this is aligned with the first hypothesis). This systematic relationship can be related with the patterns of the mean annual hydrographs.

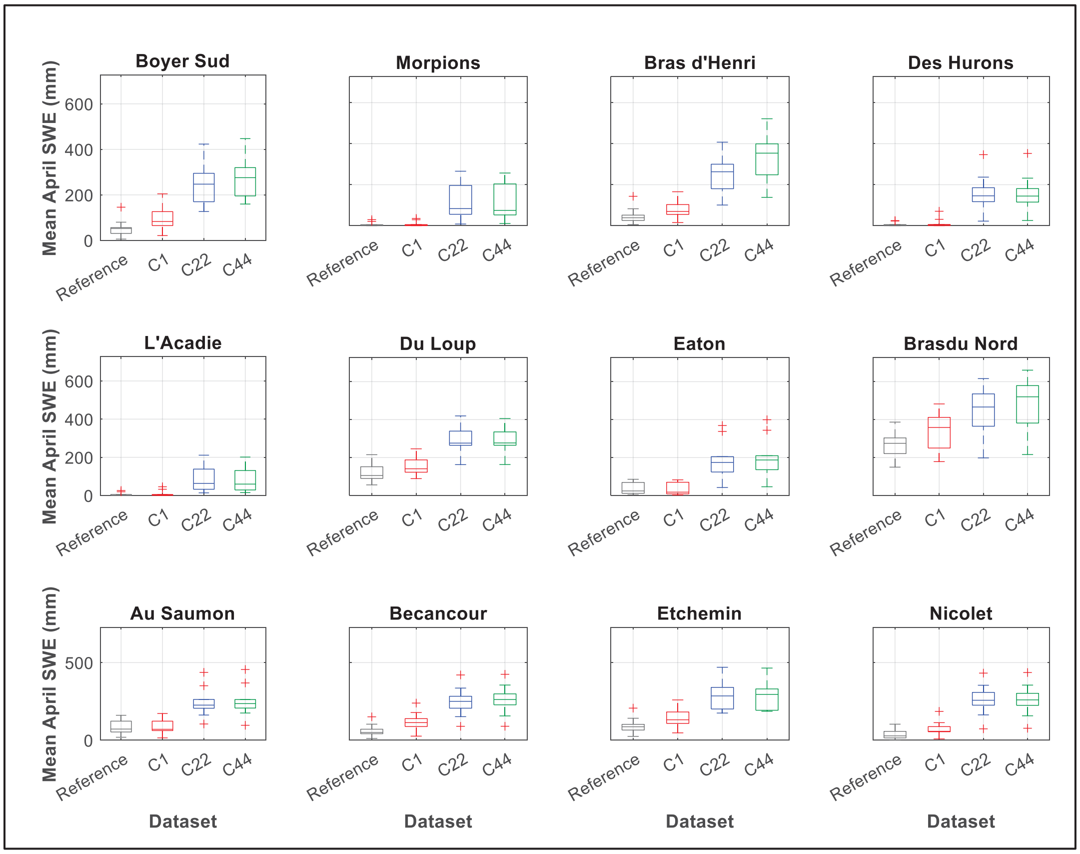


Figure 2.8 Boxplots showing the distributions of mean snow water equivalent (SWE) in April – All 12 Watersheds. Each boxplot contains ten annual values from the 2001-2010 period

### 2.5.2.3 Winter case study analysis

Figure 2.9 analyzes liquid precipitation and accumulated snowfall (Figure 2.9a), SWE (Figure 2.9b), temperature (Figure 2.9c) and streamflow (Figure 2.9d), each on a daily time scale, during the cold season from November to May, on the small representative watershed (Morpions). We performed this analysis for each of the nine seasons from 2001–2002 to 2009–2010. Noting similar patterns across all years of the simulation, we selected a specific season (2005-2006) as it represents the general behavior well. In particular, Figure 2.9a demonstrates the two different forms of simulated precipitation, liquid and solid, after CEMANEIGE-based separation according to air temperature. CONUS (C1) and Reference precipitation are mostly liquid, particularly during Nov-Dec and March-April, whereas in the CORDEX (C22 and C44) simulations, the dominant form is solid precipitation, which can lead to a larger spring freshet. In terms of simulated SWE, as shown in Figure 2.9b, all datasets show a melt episode at the beginning of December, reflected in the decline in SWE, and this is accompanied by corresponding increases in streamflow (Figure 2.9d). However, snow accumulation patterns begin to diverge in mid-December. The CORDEX simulations show higher total snow accumulation compared to the other datasets, with a larger snow water content, as shown by SWE (Figure 2.9b). By mid-March, Reference and CONUS begin to show a consistent decline in SWE, indicating the onset of snowmelt, which can be aligned with increasing rainfall events (Figure 2.9a), temperature (Figure 2.9c), and spring freshet (Figure 2.9d). The CORDEX simulations continue to accumulate snow until the end of March with slight melting episodes, and begin to show a melting process, later at the beginning of April (Figure 2.9b). This pattern can be explained with CORDEX0.44 temperature values (Figure 2.9c) remaining below zero during this period. While an earlier decline in SWE, as demonstrated by both CONUS and Reference, resulted in an initial gap. Once this gap started, neither CONUS nor Reference was able to regain the level of snow accumulation observed in the CORDEX simulations. In contrast, the two CORDEX simulations continued to accumulate snow throughout the winter, resulting in a higher overall snowpack than in both CONUS and Reference.

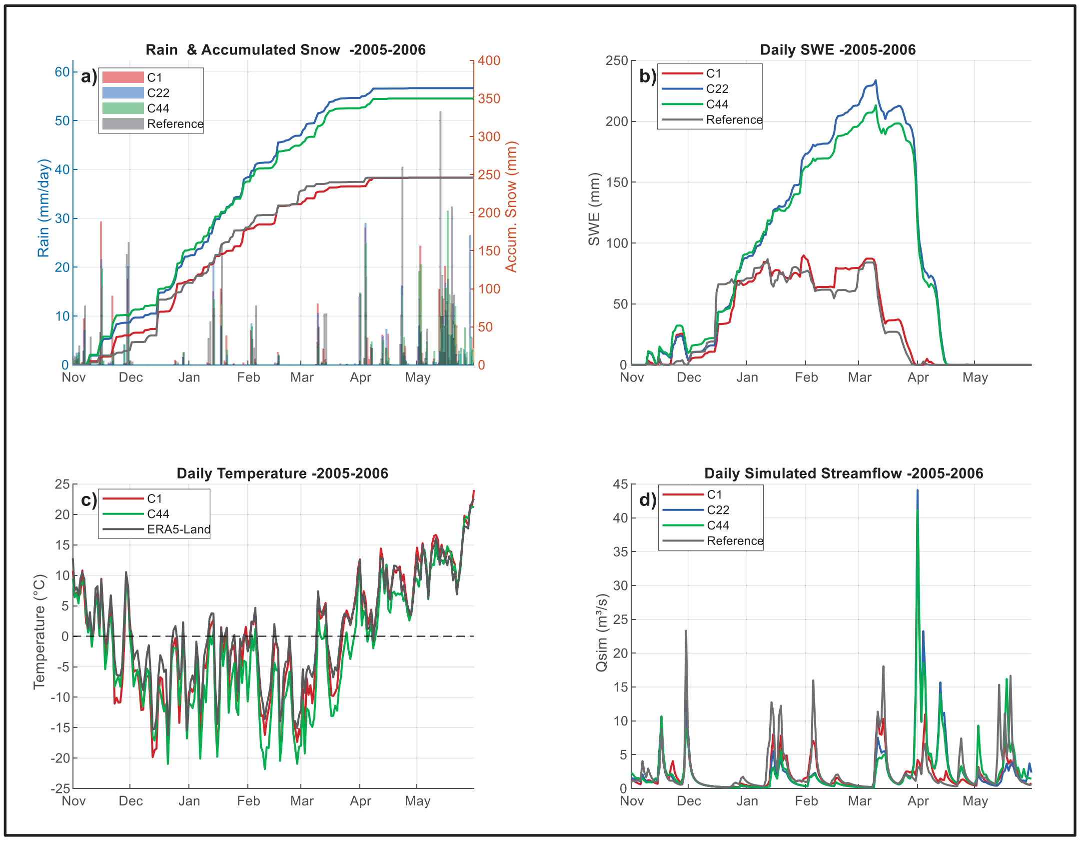


Figure 2.9 Liquid precipitation and snow accumulation (a), snow water equivalent (b), temperature (c), and streamflow (d), all on a daily time-step (November-May 2005-2006) over the small representative watershed: Morpions (surface area 94.1 km2)

#### 2.5.2.4 Bias of peak flow analysis

In order to verify our hypotheses regarding the capacity of CONUS in both spring freshet and summer-fall intense precipitation and associated floods we computed the peaks in three seasons (Apr-May-JJA-SON). Figure 2.10 presents the biases of peak streamflow against observations normalized by watershed area across three watershed size categories, including each hydrological simulation (Reference, CONUS-C1, CORDEX0.22-C22, CORDEX0.44-C44). As seen in Figure 2.10, the spread in peak bias increases as watershed size decreases, with smaller sizes showing greater inter-annual variability. However, as seen in Figure 2.6, smaller watersheds have poorer calibration results, likely due to a lack of spring freshet observations; therefore, the response may reflect a modeling product rather than a physical process. April–May stands out with the large difference among the datasets. CORDEX0.22 and CORDEX0.44 consistently show higher peak flow biases than CONUS and Reference in all three watershed categories during this season. Among large watersheds (Figure 2.10a), Reference exhibits near-zero median bias, whereas the other three datasets tend to overestimate. Medium and small watersheds categories (Figures 2.10a and 2.10b) show similar patterns, with Reference and CONUS exhibiting median biases close to zero. The near-zero median peak flow bias can be related to their earlier and lower Apr-May freshet shown in the mean hydrographs (see Figure 2.7). Conversely, CORDEX simulations generally overestimate and show a larger spread, which can be attributed to their higher mean streamflow, and to their snowmelt process (Figures 2.7 and 2.8).

During summer (JJA), the spread in peak flow bias is generally reduced compared to April-May. The large watersheds category (Figure 2.10a) shows the lowest variability, with the datasets clustering around a slightly negative median bias, suggesting a tendency to underestimate peak flows, except for CORDEX0.44. In the medium watersheds category (Figure 2.10b), CORDEX simulations show a near zero to positive median, while Reference and CONUS retain their negative median bias, as in the large watersheds. The small watersheds category (Figure 2.10c) shows the largest spread in peak bias driven by CORDEX simulations which is in accordance with mean hydrograph analysis (Figure 2.7), while CONUS and Reference continue to underestimate.

In fall (SON), bias spreads are relatively small in large and medium watersheds (Figures 2.10a and 2.10b) for all datasets, with all three simulations showing negative bias. However, in the small category (Figure 2.10c), peak flow bias spreads are again larger across all datasets. Reference consistently shows a distinct pattern compared to the other datasets, with its median remaining above zero across all three categories, indicating its higher RX1-hour values during this season (Figure 2.5b). CONUS consistently underestimates flows across all sizes. Based on this analysis, the first hypothesis regarding insignificant differences across simulations in representing the spring freshet can be rejected. Part of the second hypothesis is not verified as CONUS does not generally indicate heavier summer-fall simulated flood distribution in any of the watershed's categories.

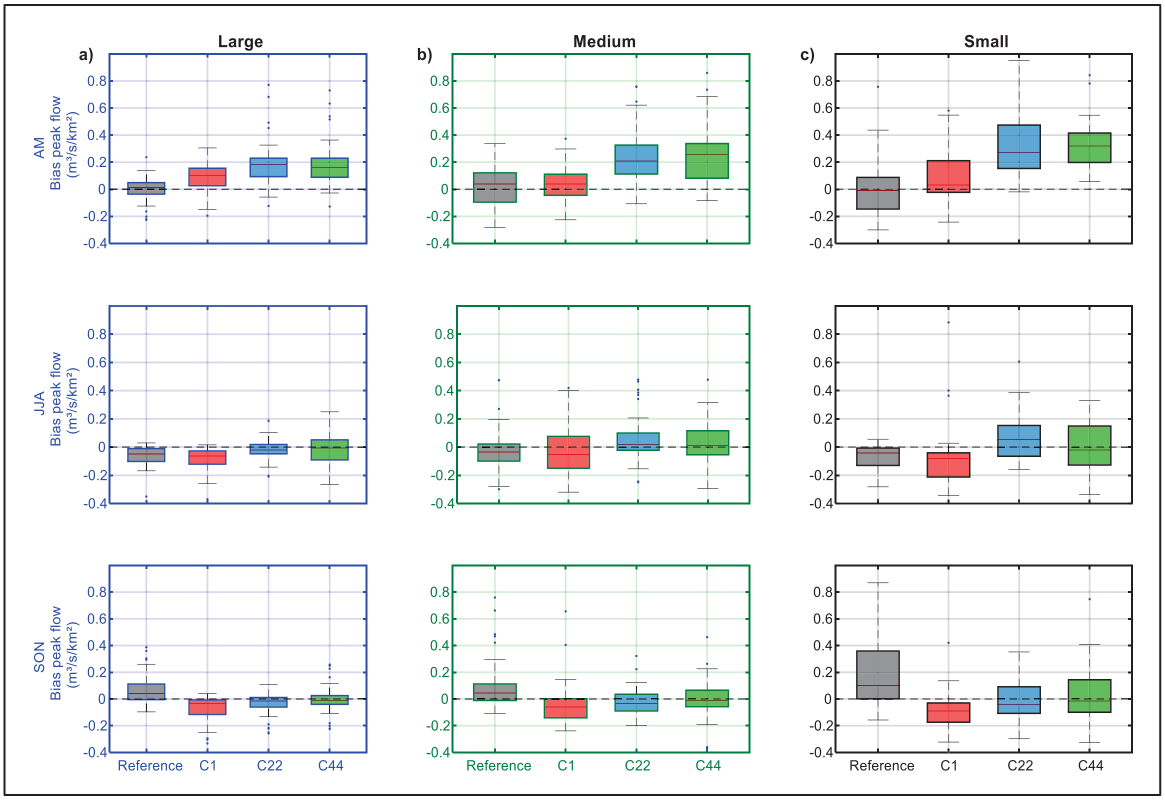


Figure 2.10 Seasonal peak streamflow biases across three watershed size categories, including each hydrological simulation (Reference, CONUS (C1), CORDEX0.22 (C22) and CORDEX0.44 (C44)), compared to observations, normalized by watershed area ($m^3/s/km^2$). a) Blue: Large category, b) green: medium category, c) black: small category. Seasons Analyzed: AM (Apr–May), JJA (Summer), SON (Fall)

### 2.5.2.5 Event-based analyses

In the following, we investigate more deeply two isolated high-intensity, short-duration precipitation events from the CONUS (C1) simulation, both of which occurred during the summer in the same watershed (Morpions). This analysis aims at identifying localized, short-duration, high-intensity precipitation events to verify the second hypothesis, whether the CPM (CONUS) captures such events, and subsequently assess the corresponding hydrological response in terms of streamflow in a small watershed. The first high-intensity rainfall event occurred on June 22, 2001, at 23:00 (Figure 2.11a), and the second one on June 9, 2007, at 05:00 (Figure 2.11b). Both selected rainfall events are the two highest storms extracted from the high-resolution CONUS (C1) simulation time series. We examined precipitation and streamflow time series over a 3-day window (72-time steps) centered on each rainfall event date, including responses from the CORDEX (C22 and C44) simulations for the small watershed (Morpions). As shown in Figure 11a, during the first event, CONUS produced a distinct and intense precipitation exceeding 25 mm/hr, which was not observed in the CORDEX0.22 and CORDEX0.44 simulations. Within a few hours, a sharp, immediate increase in CONUS-driven streamflow also appears, demonstrating a short-duration discharge response. In contrast, CORDEX0.22 and CORDEX0.44 simulations exhibited much weaker or nearly absent precipitation during this specific period and consequently failed to reproduce the noticeable rise in streamflow. The second event had the most intense short-duration precipitation among all simulations (Figure 2.11c), with the CONUS simulation producing a strong precipitation surpassing 30 mm/hr (Figure 2.11b). Simulated streamflow driven by CONUS increases significantly and instantly after this event, reaching a simulated flow of over 45 $m^3/s$ in a few hours. However, during this window period, no comparable rainfall intensity was observed by any of the two CORDEX simulations. These simulations produced only small amounts of rainfall, and no significant streamflow response. The maps (Figure 2.11c and Figure 2.11d) show the spatial extent of absolute rainfall values on the corresponding dates extracted directly from three climate outputs. We clearly observe intense rainfall driven by the convection-permitting WRF model, while this event is not evident in either of the CORDEX-driven simulations. Thus, part of hypothesis 2 can be verified by the results provided in these case studies.

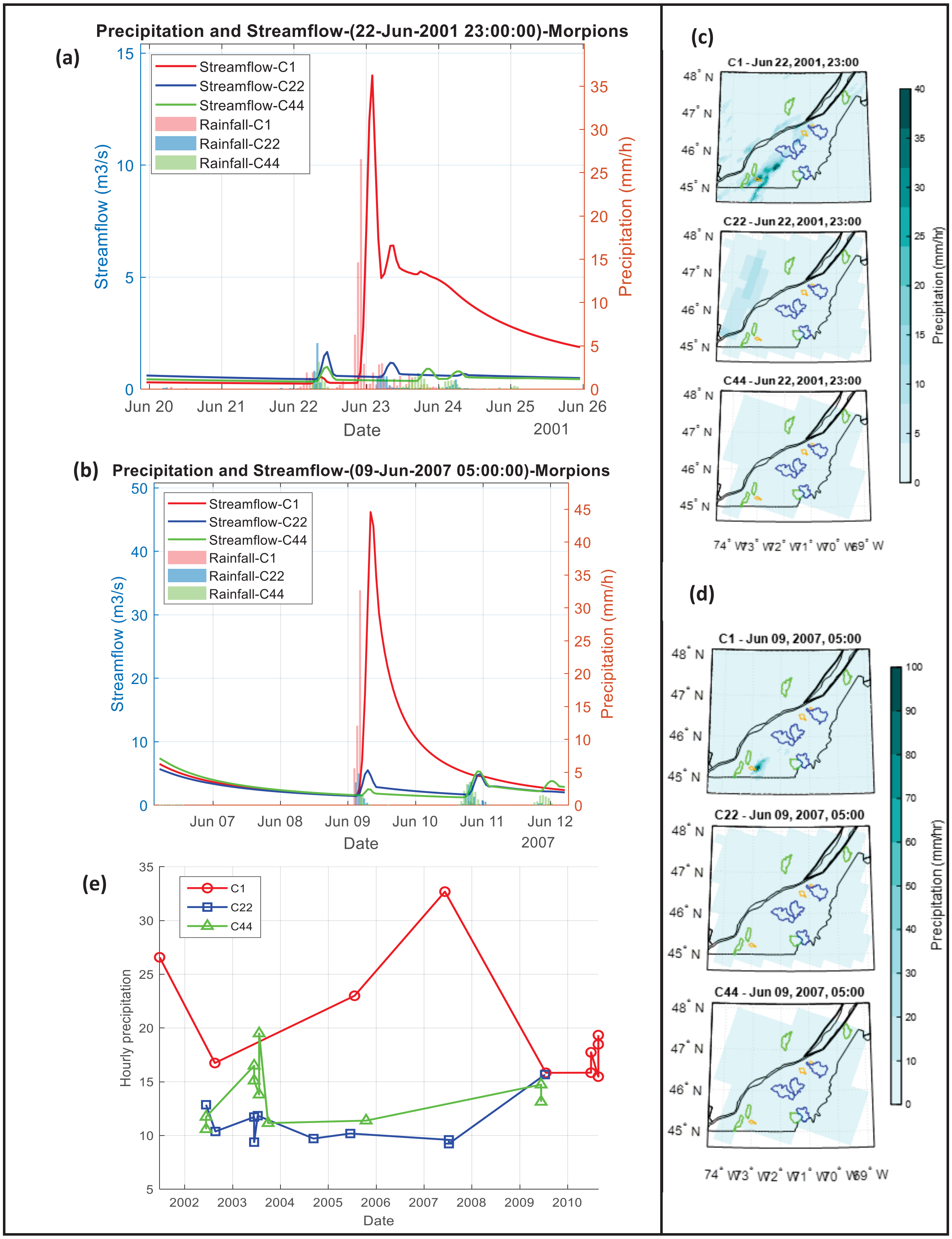


Figure 2.11 Two isolated high-intensity and short-duration CONUS (C1) precipitation events and their corresponding streamflow responses in the small watershed (a,b), with spatial extent of the rainfall on the corresponding specific dates (c,d), first10 mean maximum precipitation extracted among all three simulations CONUS (C1), CORDEX0.22 (C22) and CORDEX0.44 (C44) (e)

## 2.6 Discussion

This work presents a framework to compare outputs from three WRF regional climate model simulations (CONUS, CORDEX0.22 and CORDEX0.44) at different spatial resolutions, 4, 25 and 50 km respectively, and is organized into two levels: 1) Precipitation and temperature evaluations; 2) Hydrological modelling and evaluations, with a focus on mean annual hydrograph, simulated snow accumulation and melt, streamflow peaks bias, and specific heavy rainfall-streamflow events.

### 2.6.1 Seasonal-based meteorological comparisons

On a seasonal basis, we found that CONUS simulation generally stands with lower mean summer precipitation, and with the higher mean temperature throughout the three evaluated seasons (April-May, summer and fall). This may be linked to the systematic warmer and drier bias reported in CONUS simulation during the summer, as identified by Liu et al. (2017) over central North America. Based on this study, multiple attempts have been made to reduce this bias through physics modifications, the use of different land surface models (LSMs) and boundary layer schemes, and the exclusion of shallow convection parameterizations. However, the bias was not effectively eliminated. Yet, the study reported a reduction of at least half of the warm-season temperature bias and improved precipitation pattern simulation when spectral nudging was used (Liu et al. 2017). Simultaneously, the higher RX1-hour values of CONUS precipitation compared with other simulations indicate the influence of finer spatial resolution on the detection of short-duration intense precipitation events. This contrast can be aligned with previous findings that finer spatial resolution primarily enhances the representation of short-duration, intense rainfall events rather than seasonal means (Lucas-Picher et al. 2024). While Akinsanola et al. (2024) showed overall improvements in seasonal averages and extremes using CPMs, they also identified notable regional biases.

### 2.6.2 Seasonal-based hydrological comparisons

April–May streamflow differences across datasets indicates that temperature exerts a predominant role on flood simulation in snowmelt-driven watersheds. The higher temperature in the CONUS simulation (by ~1–2 °C relative to ERA5-Land and CORDEX0.44) can lead to earlier snowmelt and a more gradual rise in streamflow. In contrast, CORDEX simulations delay melt and concentrate runoff into sharper peaks during May. These contrasts persist into summer. Higher CORDEX spring freshet streamflow is linked to higher solid precipitation and CORDEX0.44 lower mean temperatures. A few CONUS and Reference-driven peaks during summer and fall in the mean annual hydrograph (Figure 2.7) in the small watershed (Morpions) can indicate their capacity to produce short-term, localized heavy precipitation events. In the case of the CONUS simulation, this can likely be explained by the higher resolution and more realistic representation of convective events from the higher resolution WRF model version, especially during summer and fall. The two CORDEX coarser resolutions yield a smoother hydrograph.

The lower SWE in Reference and CONUS (Figure 2.8) is consistent with their earlier and lower spring freshet (Figure 2.7). This behaviour is driven by higher April–May temperatures that promote earlier snowmelt or a shift from snowfall to rainfall. Conversely, the higher SWE in the CORDEX simulations reflects lower April-May temperatures, delaying melt and producing delayed and more significant streamflow peaks.

The results of specific daily analysis from November to May (Figures 2.9a and 2.9d) allow us to deeply analyze why a large difference occurred in Apr-May.  Subtle differences in daily temperature, drive significant changes in snowfall or rainfall, as well as meltwater generation. Given the equation of the rain/snow separation that is applied in the hydrological model, all precipitation is treated as rain when the temperature is above 3.6 °C, and all precipitation is considered snow when the temperature is below 0.6 °C. Between 0.6 °C and 3.6 °C, liquid and solid precipitation are mixed and the proportions are established based on a linear method (Kienzle 2008). In the case of CORDEX simulations, temperatures often remain below zero degree throughout the winter and early April-May, resulting in continued snow accumulation and delayed melt. In contrast, Reference and CONUS temperatures reach above-freezing earlier, leading to earlier snowmelt events occurring in March (Figure 2.9b). Besides, the rainfall in March and April indicates temperatures are high enough to produce rain or contribute to meltwater generation. Then, these early melt episodes observed in the Reference and CONUS create a lasting divergence in snowpack evolution. Even though these two datasets continue to accumulate snowfall throughout the winter, the initial (Figure 2.9c) melt episode in mid-December prevents them from regaining the higher snowpack levels as in CORDEX. So, the first hypothesis can be rejected based on the two analyses above (SWE and specific daily analysis of November-May).

The bias of peak flow patterns was established using all 12 watersheds, grouped by watershed size (Figure 2.10). Despite this aggregation, they can still be reflected in the behavior of the datasets observed in the mean annual hydrographs (Figure 2.7). During summer, the generally negative median peak biases from CONUS can be related to the effect of higher temperatures during this season. This means higher temperature leads to increased simulated evapotranspiration, resulting in less water available for streamflow. It is interesting that, in terms of mean precipitation, we found quite similar values across all datasets during this season. Although the highest RX1-hour values are reached during summer, these do not systematically extend into higher peak streamflow in this season. This has been shown in some hydroclimatic modelling studies that improvements in precipitation extremes did not consistently yield higher flood peaks (Reszler, Switanek, and Truhetz 2018; Xie, Li, Chen, and Xu 2025). In the fall, a larger spread in small watersheds is expected and is linked to their inherent sensitivity to localized rainfall events during this transition season. The consistent overestimation of Reference-driven peak bias in fall across all watershed categories can be explained by IMERG’s higher RX1-hour precipitation values during this season (Figure 2.5b). This overestimation has been shown in previous studies (Seo, Quintero, and Krajewski 2023; Woods et al. 2023; Moazami and Najafi 2021). For example, Moazami and Najafi (2021) showed that IMERG tends to overestimate precipitation intensity. Woods et al. (2023) reported an overestimation of flood duration, and Seo, Quintero, and Krajewski (2023) results showed that streamflow simulations driven by IMERG lead to overestimated discharge.

Sabzipour et al. (2025) previously showed that a 2.5 km CPM improves the simulation of intense summer-fall hourly rainfall events in southern Quebec, and that this added value translates into reduced bias in simulated peak flows for small watersheds compared to a 12 km RCM. It should be noted that a distinct setup was used in this study, including a 12 km version (CRCM6/GEM5-12km) and a convection-permitting 2.5 km version (CRCM6/GEM5-2.5km). The CRCM6/GEM5 is the sixth generation of the Canadian RCM, based on the Global Environmental Multiscale model (GEM5), which serves as an operational numerical weather prediction model (Sabzipour et al. 2025). The 12 km simulation was driven by ERA5 reanalysis at its boundary layers, while the 2.5 km simulation was driven by hourly outputs from the CRCM6/GEM5-12km simulation. The present experiment relies on the outputs from different versions of the WRF model, all forced by the same ERA-Interim reanalysis

### 2.6.3 Event-based analysis (two case studies)

Regarding the intense short-duration rainfall events analysis conducted in the small watershed (Morpions) (see Figure 11), we also tried to identify such events in CORDEX0.22 and CORDEX0.44 precipitation time series. Still, their corresponding values were much lower than in CONUS, and the desired events could not be found (Figure 2.11e). The impulsive hydrological responses driven by CONUS did not exist in CORDEX-driven hydrological simulations, meaning that CORDEX0.22 and CORDEX0.44 missed the events entirely or significantly underestimated their intensity. This is especially important in the small, and flashier watershed (Morpions), where just a single hour of intense rainfall can drive a rapid streamflow response (30–50 $m^3/s$). These findings are associated with RX1-hour, which shows that CONUS does produce heavy rainfall events, and it can still show higher peaks. The ability to simulate such localized events is especially critical for flood risk assessments in small catchments, where even single-hour rainfall events can drive rapid hydrological responses.

We need to clarify that this setup can provide a relatively fair comparison as all three climate simulations use the WRF model forced by the same reanalysis dataset (ERA-Interim) allowing the effects of spatial resolution to be examined. However, differences in Model Versions (3.4.1 for WRF 4 km horizontal grid spacing and 3.5.1 for CORDEX-NA simulations) may introduce additional limitations. These results are consistent with those that show CPM models are capable of reproducing localized convective storms that can directly cover a large portion of a small watershed with impulse runoff (Prein et al. 2015; Poncet et al. 2024). Thus, hypothesis 2 can be supported by these results, indicating that CPMs are able to simulate intense summer precipitation and associated floods than the other coarser datasets, in the small-scale watershed.

To our knowledge, our study provides the first comparison and evaluation of the abilities of three WRF ERA-Interim reanalysis-driven climate outputs at three spatial resolutions in simulating simulated discharge and flood events of southern Québec watersheds, despite remaining uncertainties regarding the benefits of CPMs.

This study has some limitations that should be acknowledged:

1- For this study, we utilized gridded reanalysis (ERA5-Land) and satellite-based products (IMERG) as our reference data due to the limited availability of station-based precipitation data across the region over the evaluated period. This could constrain comparisons across different climate simulations and affect the performance of the hydrological model.

2- The hydrological analysis was limited to a 10-year period (2001–2010). While it is sufficient to emphasize systematic differences between the three climate simulations, this timeframe is relatively short for characterizing long-term variability and extreme event frequency.

3- Two intense event-based comparisons were conducted based on the fact that the CPM version of WRF should normally be able to provide some short-duration heavy rainfall events that we normally would not expect to find in the CORDEX 0.22 and 0.44 simulations. However, the lack of observed datasets prevented a perfect event-by-event comparison.

4- The GR5dt lumped model cannot explicitly capture spatial heterogeneity. This can limit its ability to fully translate sub-daily precipitation produced by the 4 km WRF model into peak flows.

5- The conceptual nature of GR5dt involves that PET and snow processes modelling are temperature-based, which has a direct impact on hydrological simulation results.

## 2.7 Conclusion

This study evaluated how three climate ERA-Interim-driven simulations from WRF RCM at different spatial resolutions represent heavy precipitation and how these differences extend into hydrological modeling across three different seasons (Apr-May-JJA-SON). We ran the GR5dt hydrological model across twelve watersheds in southern Québec using a convection-permitting simulation (CONUS) and two coarser WRF regional climate model simulations (CORDEX) and investigated two hypotheses: 1) All three WRF simulations can demonstrate similar patterns during the spring freshet. 2) The high-resolution WRF simulation can show benefits compared to coarser-resolution WRF simulations in terms of summer and fall storms. The key findings of each hypothesis are the following:

1. The mean annual hydrograph shows distinct differences among the simulations, particularly during spring freshet (Apr-May) (Figure 2.7). SWE results can validate the different behaviors between the high-resolution (CONUS) and coarser (CORDEX0.22 and CORDEX0.44) resolution WRF model simulations (Figure 2.8). Higher temperatures in the CONUS simulation (Figure 2.4) can lead to earlier melting, lower values of the mean snow water equivalent (SWE) and result in lower April–May flows. Thus, these findings do not support the first hypothesis.

2. The RX1-hour analysis shows that during summer (Figure 2.5a), the high-resolution WRF simulation shows more intense RX1-hour values than the other two WRF simulations, while seasonal peak-flow biases (Figure 2.10) show that the CONUS simulation underestimated summer peaks. Hence, part of the second hypothesis, related to summer peak flow bias, is not supported. In contrast, event-based analysis in Figure 2.11 shows intense rainfall events driven by the convection-permitting WRF simulation, whereas these events are not evident in either of the WRF model CORDEX simulations. Therefore, this finding supports the part of the second hypothesis regarding the representation of intense summer rainfall events and their associated flooding in the small watershed.

Given the conclusions, the future work would include:

A bias correction step is required for accurate flood predictions or operational experiments, even when driven by CPMs.

Future work could extend this analysis by incorporating other hydrological modeling approaches, such as distributed and physically-based models.

The development of long-term and even larger ensembles of CPM simulations is recommended to better assess the robustness of the added value of CPMs for hydroclimatic and hydrological impact assessments.

## 2.8 Funding

This research was supported by the Marcelle Gauvreau Engineering Research Chair in Impacts of environmental changes on watersheds' hydrology at École de technologie supérieure (ÉTS) and by the Natural Sciences and Engineering Research Council of Canada (NSERC) under Grant No. RGPIN-2020-05630.

## 2.9 Acknowledgements

We acknowledge the use of the ERA5-Land reanalysis dataset generated by Muñoz-Sabater et al. (2021). It has been downloaded from the Copernicus Climate Change Service (C3S) Climate Data Store: ('Copernicus Climate Change Service (C3S) Climate Data Store'). "*The* IMERG V6 *data were provided by the NASA/Goddard Space Flight Center's* Multi-satellite precipitation product for the U.S. GPM team *and PPS, which develop and compute the* IMERG V6 *as a contribution to GPM, and archived at the NASA GES DISC*." We gratefully acknowledge the ESCER Centre for their assistance in accessing the ERA5-Land and IMERG V6 datasets. River discharge data from hydrometric stations were obtained from the Ministère de l'Environnement, de la Lutte contre les changements climatiques, de la Faune et des Parcs (MELCCFP) and can be accessed at: https://www.cehq.gouv.qc.ca/atlas-

hydroclimatique/stations-hydrometriques/index-en.htm. This work uses high resolution WRF simulations over southern Canada archived at https://doi.org/10.5065/D6V40SXP (Rasmussen and Liu 2017), the data files are not currently publicly accessible; therefore, they will be made available upon submitting a request. The North America CORDEX (NA-CORDEX) dataset from https://gdex.ucar.edu/datasets/d316009/dataaccess/.

# APPENDIX I

## SUPPLEMENTARY MATERIAL

We obtained hourly precipitation data from weather stations across southern Québec from the Environment and Climate Change Canada (ECCC 2025) database. Given data availability during the study period (2001–2020), we selected three weather stations to evaluate the two reference datasets (IMERG and ERA5-Land) used in this study. The data for these three stations are available from 2005 to 2019. Even though their temporal coverage (2005–2019) is not precisely consistent with that of the reference datasets used for calibration (2001–2020), they still represent the most reliable observational data available for this region. Figure A1 shows the diurnal precipitation cycle over a 15-year period. We used precipitation data from IMERG, ERA5-Land, and station observations for the summer (June to August) and fall (September to November) from 2005 to 2019.

Figure-A I-1 shows the diurnal cycle of mean hourly precipitation for 3 stations and the nearest grid point from 2 reference datasets for two seasons (JJA and SON). As we see in Figure-A I-1a and A I-1b, the observations (Riviéere-du-loup) differ from the two datasets in terms of timing, magnitude, and shape. Regarding timing, the observed values show a slight increase in precipitation during the late afternoon and evening hours, and this pattern is generally captured by IMERG, whereas ERA5-Land shows weaker temporal variation and does not clearly reproduce the timing of this increase. In terms of magnitude, both IMERG and ERA5-Land tend to produce higher precipitation values than the observed ones during the day, indicating a positive bias relative to the observations. As seen, the observed diurnal cycle shows higher variability throughout the day, with lower values in the morning and higher values later in the day. IMERG follows a pattern similar to the observations, while ERA5-Land shows a smoother pattern, suggesting reduced representation of hourly variability.

As seen in Figure-A I-1c, in summer, the station (LA Pocatiere) shows a noticeable increase in precipitation during the late afternoon and evening, which ERA5-Land partially captures.

But IMERG shows a delay with some exaggeration, particularly during the evening peak. In fall Figure-A I-1d), stations show more uniform precipitation variations throughout the day, with ERA5-Land showing a relatively consistent pattern while IMERG shows larger variations.

As seen, in terms of magnitude, both datasets generally produce higher precipitation values than the station-based values, with IMERG showing the higher overestimation during the evening hours in summer. The observations display moderate diurnal variability, particularly in summer, whereas ERA5-Land presents a smoother and flatter diurnal cycle and IMERG shows larger hourly variability. Overall, ERA5-Land tends to smooth the diurnal signal, while IMERG better represents the temporal variability but with larger magnitude.

As shown in Figure-A I-1e and A I-1f, the station-based observation (L'Assomption) shows a clear increase in precipitation during the afternoon and evening hours, with a peak around late afternoon. The peak is partly reproduced by ERA5-Land and IMERG, though the timing of the peak is smoother and shifted in both datasets, particularly in summer. While in fall the timing is weaker among the datasets, with IMERG presenting more variability. As seen, in terms of magnitude, both ERA5-Land and IMERG generally show higher precipitation values for several hours of the day, particularly in the evening. Regarding the pattern, the observed diurnal cycle shows higher variability, with a noticeable afternoon-evening peak. Whereas ERA5-Land fails to represent this peak, and IMERG shows larger fluctuations throughout the day. Overall, ERA5-Land tends to show smoother diurnal variability, while IMERG can capture hourly variability, and with larger magnitude variations relative to observations.

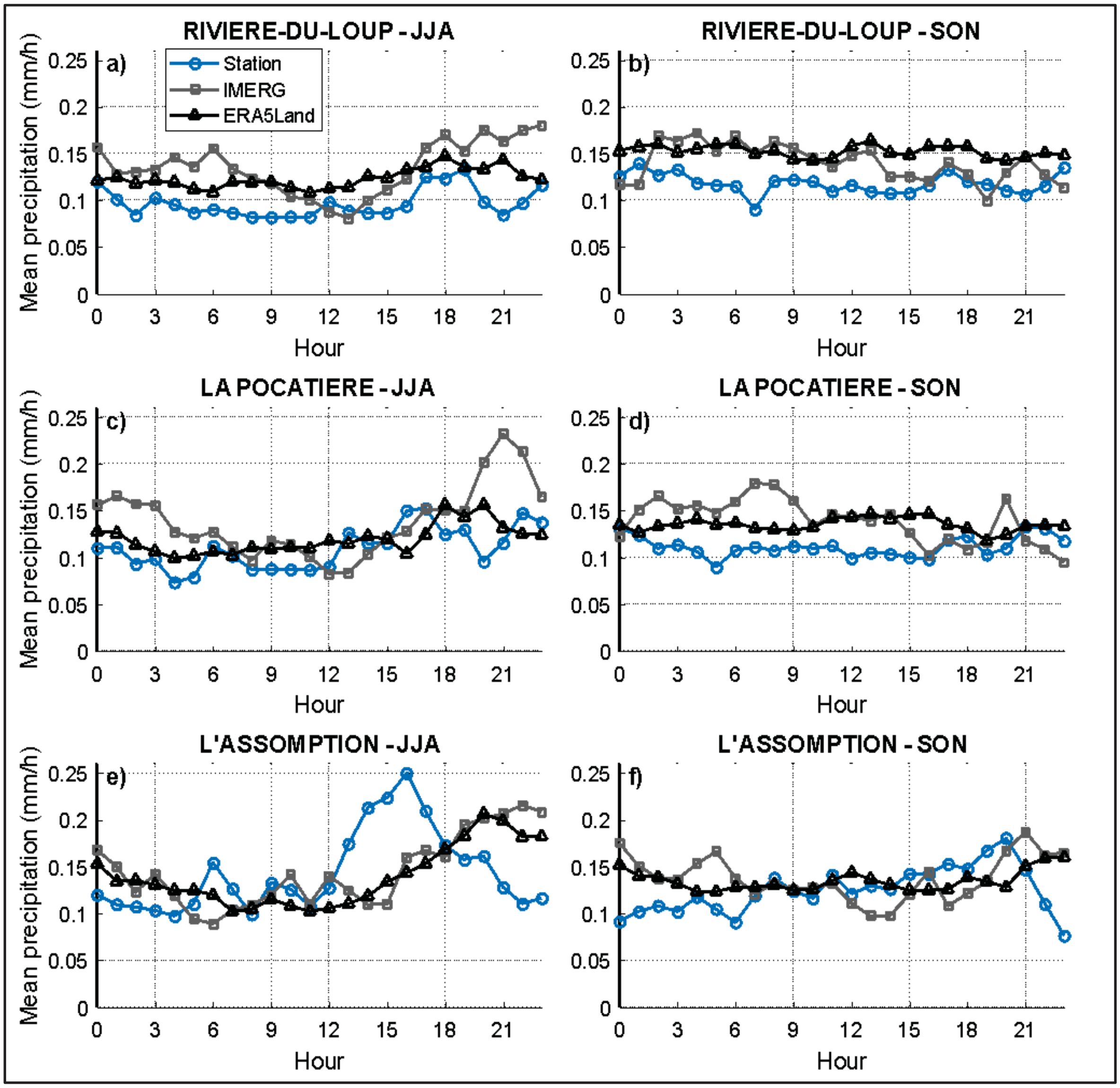


Figure-A I-1 Diurnal cycle for three stations and the closest grid point from two datasets (IMERG and ERA5Land) to each of the three stations: two seasons of Summer (JJA) and Fall (SON), across 2005-2019

We then computed the average maximum hourly rainfall events over the 15-year period (2005–2019). Figure-A I-2 shows RX1-hour presenting the spatial distribution of RX1-hour precipitation values during the summer and fall seasons across three datasets: IMERG, ERA5Land, and three representative observed stations. This analysis showed that IMERG provided a more compatible precipitation distribution with respect to stations. However, in the case of ERA5Land, a big difference is observed. This led to selecting hourly precipitation data from IMERG as our reference data for the calibration of the hydrological model.

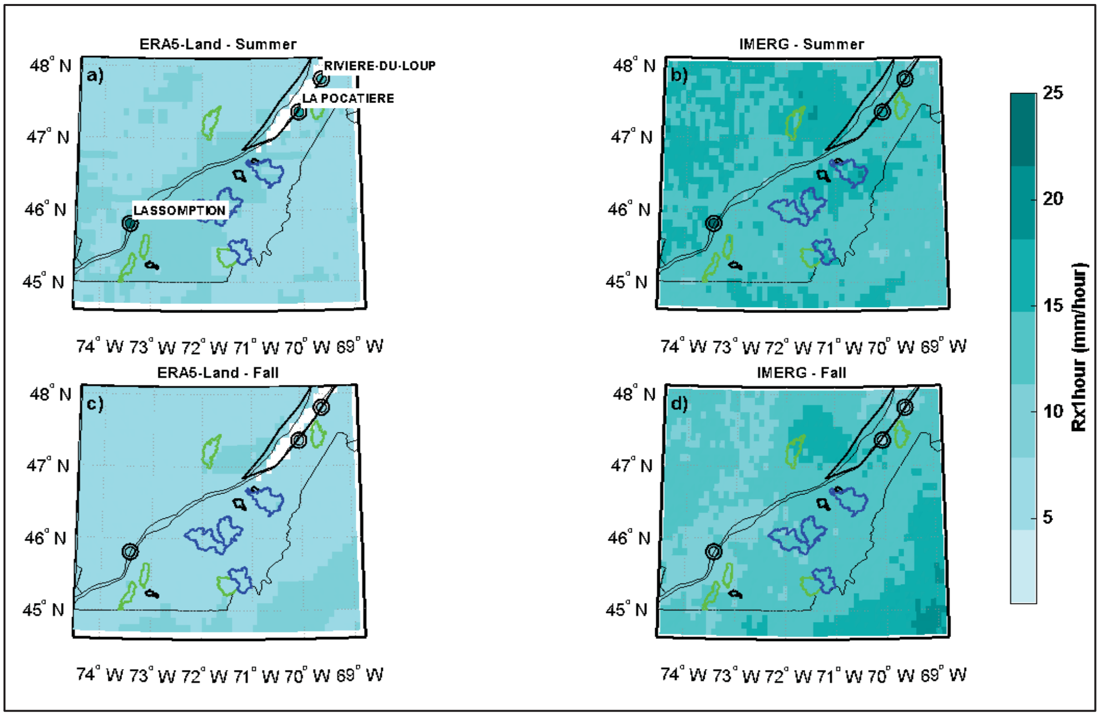


Figure-A I-2 The mean of RX1-hour for summer Era5Land on the top left (a), IMERG on the top right (b), the mean of RX1-hour for fall Era5Land on the lower left (c) IMERG on the lower right (d), with respect to the station-based data (2005-2019)

Figure-A I-3 represent liquid precipitation and accumulated snowfall (Figure A I-3a), SWE (Figure A I-3b), temperature (Figure A I-3c) and streamflow (Figure A I-3d), each on a daily time scale, during the cold season from November to May, on the large representative watershed (Becancour). Despite relative similarity in winter precipitation amounts, differences emerge in snow accumulation and spring streamflow. C22 and C44 produce higher SWE values with delayed snowmelt. This can be due to colder winter and early spring temperatures, resulting in later and sharper freshet peaks. In contrast, the higher temperature (warmer winter) in the C1 simulation results in lower SWE and earlier snowmelt which resembles the reference simulation. These results show that temperature biases exert a stronger control on spring hydrological response than precipitation differences in these snow-dominated watersheds. Figure-A I-4 shows the same analysis for the medium representative watershed (Du Loup).

Here, all 3 climate simulations reproduce the seasonal snowpack magnitude with a relatively similar pattern. However, warmer winter temperatures in the C1 (CONUS) simulation cause earlier snowmelt. Differences from May to Nov are driven more by temperature and snow processes than by precipitation totals.

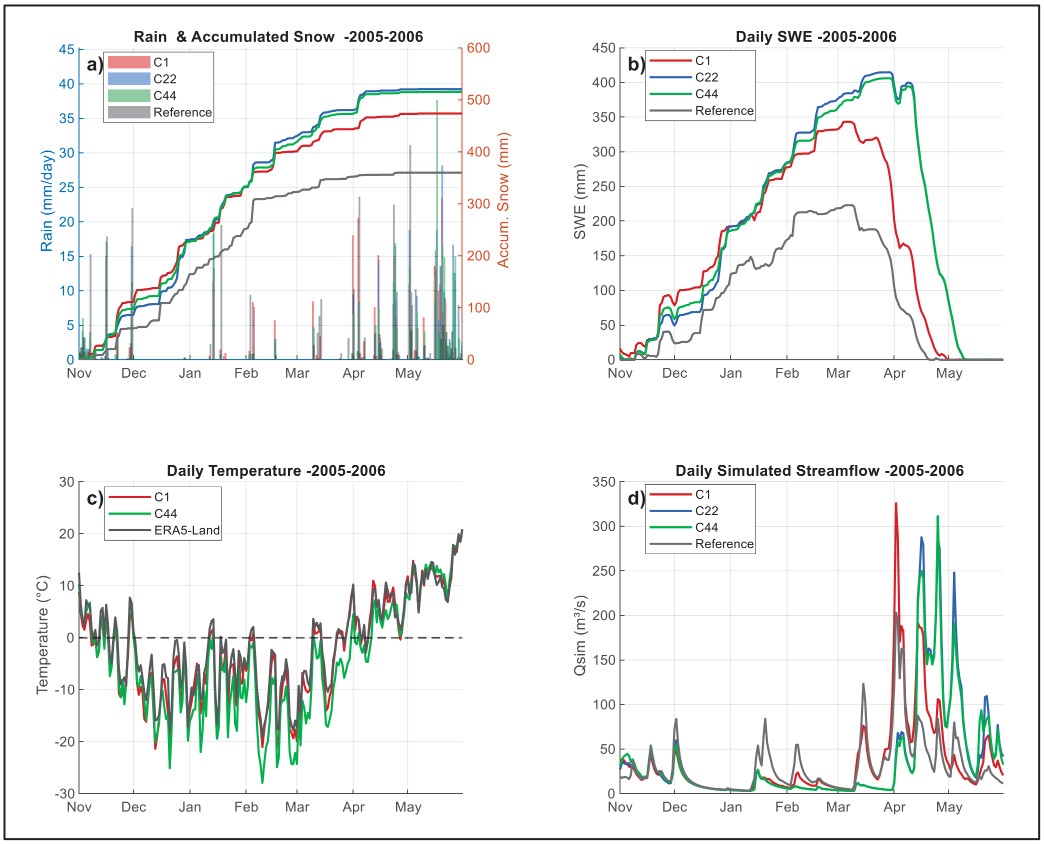


Figure-A I-3 Liquid precipitation and snow accumulation (a), snow water equivalent (b), temperature (c), and streamflow (d), all on a daily time-step (November-May 2005-2006) over the large representative watershed: Becancour (surface area 914 km2)

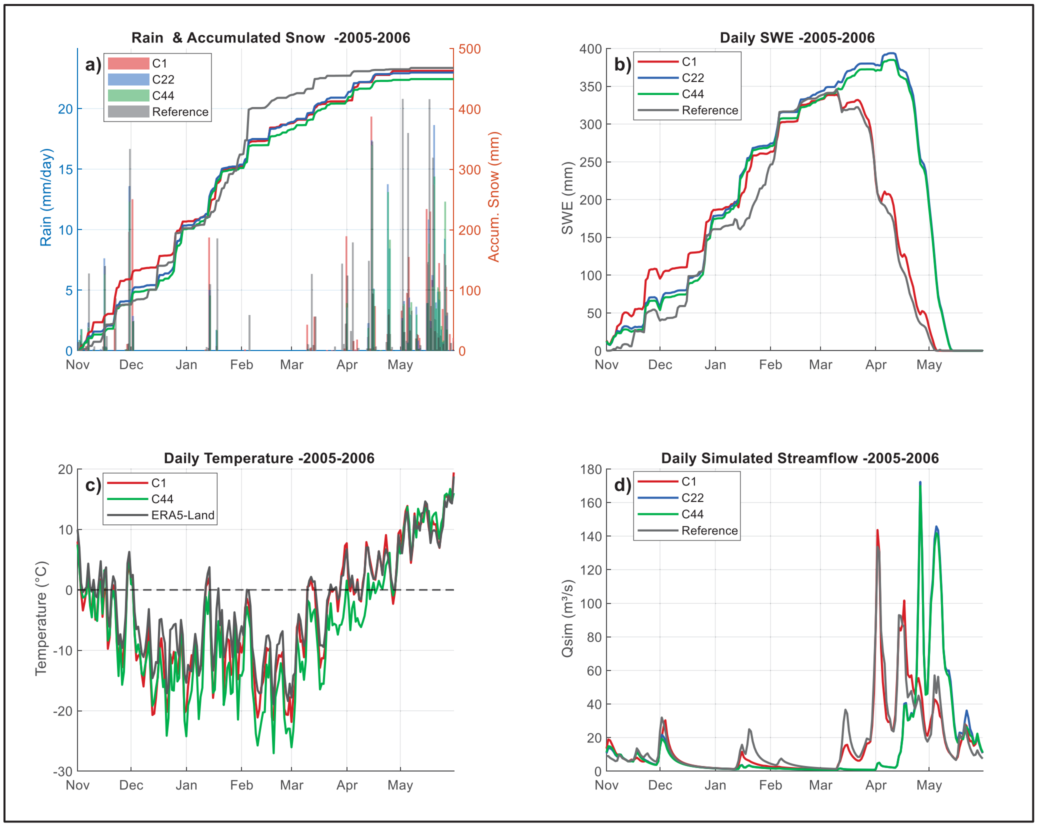


Figure-A I-4 Liquid precipitation and snow accumulation (a), snow water equivalent (b), temperature (c), and streamflow (d), all on a daily time-step (November-May 2005-2006) over the medium representative watershed: Du Loup (surface area 515 km2)

We further examined seasonal peak-flow biases (normalized by watershed area) for each of the twelve watersheds separately, in order to analyse how each watershed behaves with respect to each of the three climatic forcing (Figure-A I-5). As can be seen in this figure, each watershed generally shows a similar pattern as in Figure 2.10. In large watersheds (the first four figures from the top), peak-flow biases are generally small and closely spread, indicating rather limited sensitivity to precipitation resolution. During April–May, CORDEX0.22 and CORDEX0.44 consistently show positive biases, indicating higher spring peak flows generated by larger snowmelt. CONUS and Reference show lower or almost no bias, consistent with their lower snow water equivalent and earlier snowmelt timing. In summer and fall, all datasets remain closer to zero bias, and variability is reduced.

In medium-sized watersheds, we can see that model simulations begin to diverge more noticeably across datasets and seasons. CORDEX simulations continue to show overestimated spring peaks, while CONUS and Reference remain closer to observed magnitudes. In contrast, during summer, peak-flow biases exhibit a wider spread and often have negative medians, except for a medium watershed (Brasdu Nord). Fall responses remain moderate, though Reference shows a slight positive shift.

The largest contrast occurs in small watersheds, which show strong sensitivity to the climate forcing. CORDEX simulations systematically overestimate April–May peak flows, which is consistent with their lower temperatures, increased snow accumulation, and delayed melting. CONUS and Reference generate almost zero or slightly positive medians. In the summer, two CORDEX simulations exhibit generally positive or near-zero medians, except for CORDEX0.44 in the smallest watershed (Boyer Sud). CONUS and Reference remain negative, indicating underestimation of runoff peaks, despite CONUS showing the highest mean RX1-hour precipitation. The variability remains significant in fall, particularly for Reference, reflecting increased uncertainty in local precipitation for small, flashy systems.

Overall, regarding peak flow bias, the smaller, fast-responding watersheds tend to show a broader distribution of peak bias, while large watersheds tend to reduce it. This means that, regardless of the spatial resolution of the three climate outputs, the scaling effect can be observed consistently across all datasets. This is because hydrological modelling is inherently more sensitive in smaller watersheds.

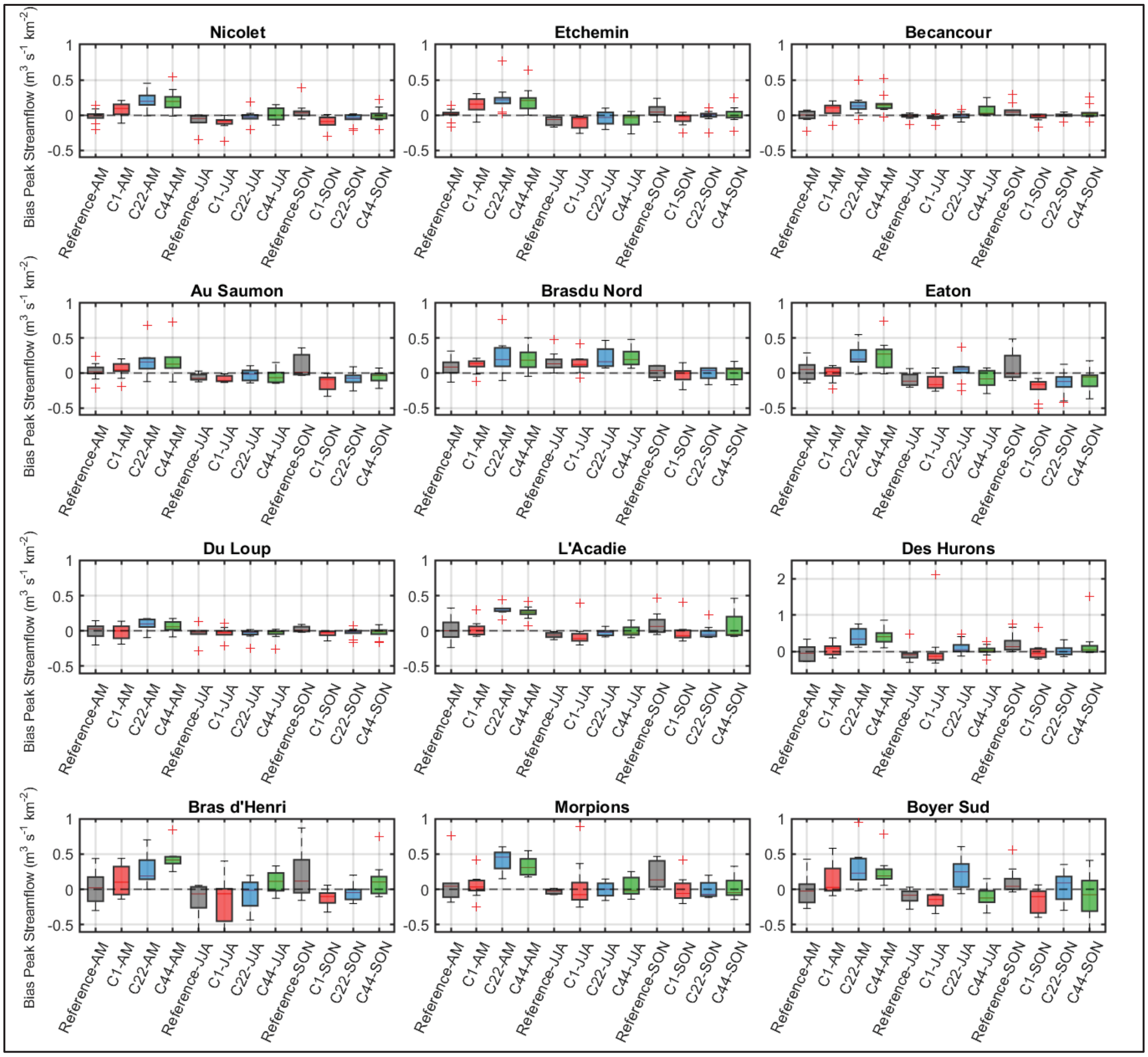


Figure-A I-5 Seasonal peak streamflow biases across all 12 watersheds, with each dataset shown in a specific color (Reference (gray), CONUS (red), CORDEX22 (blue), CORDEX44 (green)), compared to observations, normalized by watershed area ($m^3/s/km^2$). 3 Seasonal Analyses: AM (April-May), JJA (Summer), SON (Fall)

Figure-A I-6 shows the mean seasonal higher potential evapotranspiration (PET), including each climate simulation (CONUS, CORDEX22 and CORDEX44) across three watershed size categories. In general, C1 produced higher potential evapotranspiration (PET) than C22 and C44 across all three seasons, although it is typically lower during April–May (AM) and fall (SON). Although CONUS (C1) generates more intense summer rainfall, higher temperatures likely increase potential evapotranspiration and reduce the amount of water available for runoff generation. Therefore, the increased summer potential evapotranspiration can explain why the higher precipitation extremes simulated by CONUS C1 did not consistently translate into higher peak streamflow.

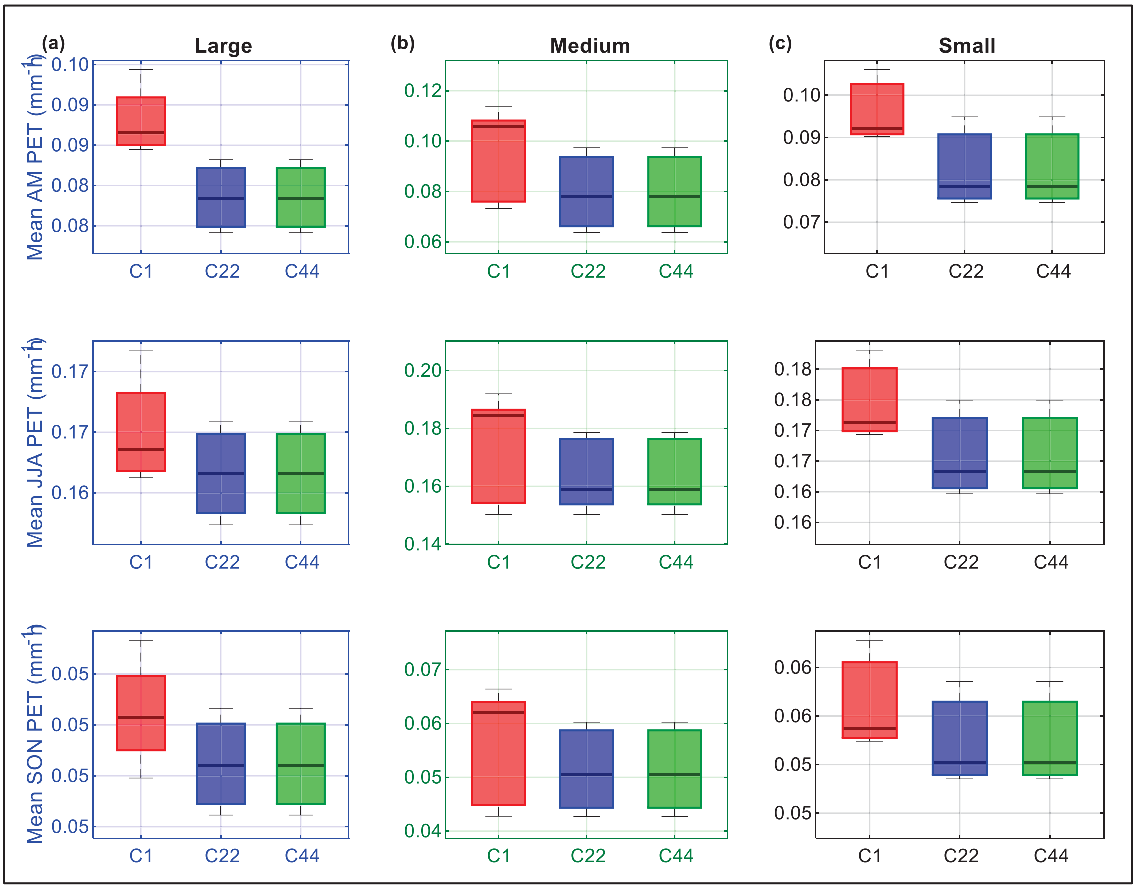


Figure-A I-6 Mean seasonal PET, including each climate simulation shown in a specific color (CONUS (red), CORDEX22 (blue), CORDEX44 (green)), across three watershed size categories: a) Large, b) Medium, and c) Small, across 3 seasons including AM (April-May), JJA (Summer), SON (Fall)

Figure-A I-7 shows that CONUS (C1) produced the higher mean hourly precipitation values, with a higher median and larger variability than the two CORDEX simulations (C22 and C44). The presence of higher outliers in C1 can indicate its tendency to generate more intense precipitation events in the small-scale watershed category. In comparison, C22 and C44 generally generate lower precipitation values, with C44 producing the lowest values, likely reflecting its coarser spatial resolution.

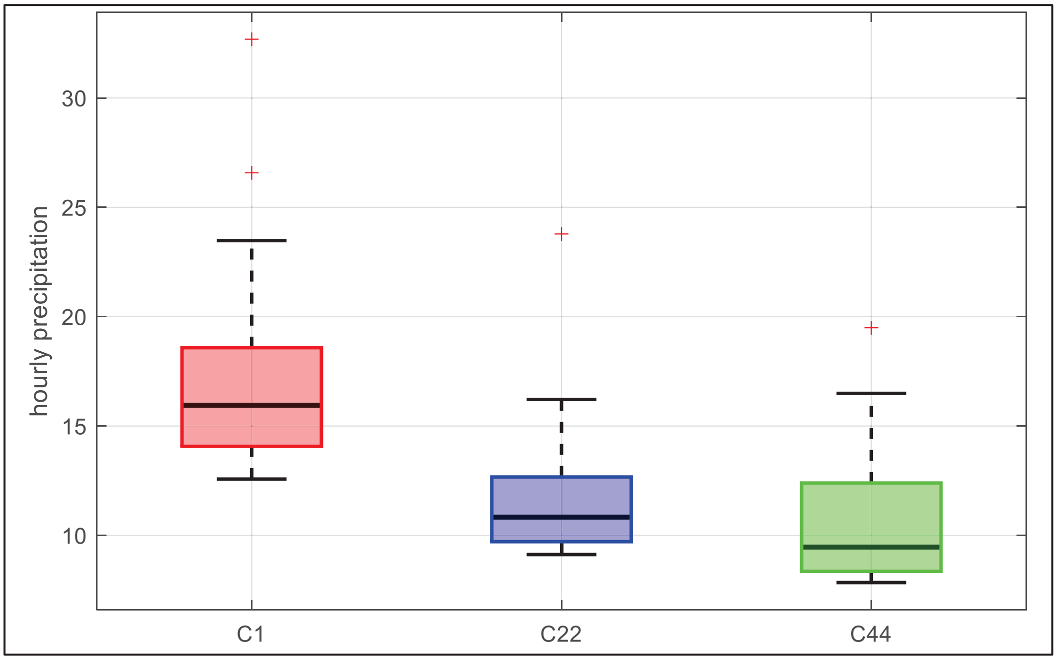


Figure-A I-7 Distribution of the first 10 mean maximum precipitation values during summer and fall (Jun-November) extracted across all three simulations CONUS (C1), CORDEX0.22 (C22), and CORDEX0.44 (C44), over the category of small representative watersheds (Boyer Sud (61 km²), Morpions (94.1 km²), Bras d'Henri (154 km²))

## CONCLUSION AND RECOMMENDATIONS

In this study, we evaluated the performance of three hourly WRF regional climate model simulations: a convection-permitting simulation (High-Resolution CONUS) against two coarser-resolution simulations (CORDEX22 and CORDEX44) that use convective parameterization. We focused on mean precipitation and heavy precipitation, as well as mean temperature, across a study domain located in southern Québec. We further examined the performance of these three hourly WRF model simulations in reproducing flood peaks, using a conceptual hydrometeorological model (GR5-dt) for comparison. The main conclusions from this study are as follows:

1. The results of April–May mean streamflow pattern and SWE across WRF simulations highlights significant differences in snowmelt timing and spring flood. CONUS simulation with higher temperatures is likely to lead to earlier snowmelt during spring freshet, as reflected in the gradual earlier rise in CONUS-driven streamflow in the mean hydrograph. CONUS higher temperatures directly influence the differences in the April/May streamflow behaviour. Thus, the findings can reject the first hypothesis.

2. Although High-resolution climate simulations (CONUS) highlight the ability of the model in producing localized extremes in precipitation, particularly during the summer, this performance does not consistently extend into higher summer peak flows simulations. This is mainly due to the increased simulated potential evapotranspiration because of higher temperatures in the CONUS simulation. Conversely, the event-based analysis identified a heavy rainfall event simulated by the convection-permitting CONUS simulation that is not captured by either of the CORDEX simulations. Therefore, part of the second hypothesis regarding the ability of CPM in simulating intense summer-fall precipitation and associated flooding in a small-scale watershed, can be verified in this case study.

We can draw the conclusion that resolution-related differences in climate forcing do not necessarily translate into hydrological simulations. CONUS generally provides lower streamflow peaks during summer, compared to the CORDEX simulations. However, our event-based results showed that CONUS can produce rapid, short-duration flood peaks when localized heavy rainfall occurs over the small watershed during the season when convection is most influential. Yet, this pattern does not necessarily appear in the broader seasonal evaluation.

Furthermore, the use of distributed hydrological models (such as Hydrotel) could better reflect the spatial detail of high-resolution climate forcing outputs, since spatial heterogeneity may not be represented by lumped models. A bias correction step is needed for accurate flood predictions, even when driven by CPMs.

# LIST OF BIBLIOGRAPHICAL REFERENCES


Aguilar Andrade, Freya Saima, Richard Arsenault, Annie Poulin, Magali Troin, and William Armstrong. 2024. 'Application of weather post-processing methods for operational ensemble hydrological forecasting on multiple catchments in Canada', Journal of Hydrology, 642: 131861.

Akinsanola, Akintomide Afolayan, Chunyong Jung, Jiali Wang, and Veerabhadra Rao Kotamarthi. 2024. 'Evaluation of precipitation across the contiguous United States, Alaska, and Puerto Rico in multi-decadal convection-permitting simulations', Scientific reports, 14: 1238.

Arsenault, Richard, François Brissette, and Jean-Luc Martel. 2018. 'The hazards of split-sample validation in hydrological model calibration', Journal of Hydrology, 566: 346–62.

Arsenault, Richard, Annie Poulin, Pascal Côté, and François Brissette. 2014. 'Comparison of stochastic optimization algorithms in hydrological model calibration', Journal of Hydrologic Engineering, 19: 1374–84.

Bador, Margot, Julien Boé, Laurent Terray, Lisa V Alexander, Alexander Baker, Alessio Bellucci, Rein Haarsma, Torben Koenigk, Marie-Pierre Moine, and Katja Lohmann. 2020. 'Impact of higher spatial atmospheric resolution on precipitation extremes over land in global climate models', Journal of Geophysical Research: Atmospheres, 125: e2019JD032184.

Bastola, Satish, Conor Murphy, and John Sweeney. 2011. 'The role of hydrological modelling uncertainties in climate change impact assessments of Irish river catchments', Advances in water resources, 34: 562–76.

Bélair, Stéphane, Pei-Ning Feng, Franck Lespinas, Dikra Khedhaouiria, David Hudak, Daniel Michelson, Catherine Aubry, Florence Beaudry, Marco L. Carrera, and Julie M. Thériault. 2024. 'IMERG in the Canadian Precipitation Analysis (CaPA) System for Winter Applications', Atmosphere, 15: 763.

Belušić, Andreina, Maja Telišman Prtenjak, Ivan Güttler, Nikolina Ban, David Leutwyler, and Christoph Schär. 2018. 'Near-surface wind variability over the broader Adriatic region: insights from an ensemble of regional climate models', Climate Dynamics, 50: 4455–80.

Bergström, S. 1995. "The HBV model. Computer Models of Watershed Hydrology, VP Singh, Ed." In.: Water Resources Publications.

Berner, Judith, Ulrich Achatz, Lauriane Batte, Lisa Bengtsson, Alvaro de la Cámara, Hannah M Christensen, Matteo Colangeli, Danielle RB Coleman, Daan Crommelin, and Stamen I Dolaptchiev. 2017. 'Stochastic parameterization: Toward a new view of weather and climate models', Bulletin of the American Meteorological Society, 98: 565–88.

Berthou, Ségolène, Elizabeth J Kendon, Steven C Chan, Nikolina Ban, David Leutwyler, Christoph Schär, and Giorgia Fosser. 2020. 'Pan-European climate at convection-permitting scale: a model intercomparison study', Climate Dynamics, 55: 35–59.

Beven, Keith. 2006. 'A manifesto for the equifinality thesis', Journal of Hydrology, 320: 18–36.

Beven, Keith J. 2012. Rainfall-runoff modelling: the primer (John Wiley & Sons).

Bian, Qingyun, Shu Wang, Heng Yang, and Hui Zheng. 2026. 'Intercomparison and sensitivity analysis of WRF parameterization schemes for convection-permitting modeling of precipitation distribution along the Yarlung Zangbo River', Atmospheric Research, 336: 108827.

Bouadi, Tassadit, Marie-Odile Cordier, Pierre Moreau, René Quiniou, Jordy Salmon-Monviola, and Chantal Gascuel-Odoux. 2017. 'A data warehouse to explore multidimensional simulated data from a spatially distributed agro-hydrological model to improve catchment nitrogen management', Environmental Modelling & Software, 97: 229–42.

Boville, Byron A, and Peter R Gent. 1998. 'The NCAR climate system model, version one', Journal of Climate, 11: 1115–30.

Brissette, F, R Arsenault, MA Boucher, M Braun, D Huard, M Leduc, A Poulin, and R Turcotte. 2023. 'Évolution du risque hydrologique lié aux événements pluvieux extrêmes: Application des données ClimEX (Québec-Bavière'.

Brockhaus, Peter, DANIEL Luthi, and Christoph Schar. 2008. 'Aspects of the diurnal cycle in a regional climate model', Meteorologische Zeitschrift, 17: 433–44.

Chen, Hanqing, Bin Yong, Pierre-Emmanuel Kirstetter, Leyang Wang, and Yang Hong. 2021. 'Global component analysis of errors in three satellite-only global precipitation estimates', Hydrology and Earth System Sciences, 25: 3087–104.

Chen, Jie, François P Brissette, Annie Poulin, and Robert Leconte. 2011. 'Overall uncertainty study of the hydrological impacts of climate change for a Canadian watershed', Water Resources Research, 47.

Christensen, Jens Hesselbjerg, and Ole Bøssing Christensen. 2007. 'A summary of the PRUDENCE model projections of changes in European climate by the end of this century', Climatic change, 81: 7–30.

'Copernicus Climate Change Service (C3S) Climate Data Store'. https://cds.climate.copernicus.eu/datasets/reanalysis-era5-land.

Coppola, Erika, Stefan Sobolowski, E Pichelli, F Raffaele, B Ahrens, I Anders, N Ban, Sophie Bastin, Michael Belda, and D Belusic. 2020. 'A first-of-its-kind multi-model convection permitting ensemble for investigating convective phenomena over Europe and the Mediterranean', Climate Dynamics, 55: 3–34.

Dallan, Eleonora, Marco Borga, Giorgia Fosser, Antonio Canale, Bardia Roghani, Marco Marani, and Francesco Marra. 2024. 'A method to assess and explain changes in sub-daily precipitation return levels from convection-permitting simulations', Water Resources Research, 60: e2023WR035969.

Dallan, Eleonora, Francesco Marra, Giorgia Fosser, Marco Marani, Giuseppe Formetta, Christoph Schär, and Marco Borga. 2023. 'How well does a convection-permitting regional climate model represent the reverse orographic effect of extreme hourly precipitation?', Hydrology and Earth System Sciences, 27: 1133–49.

Denis, B, R Laprise, and D Caya. 2003. 'Sensitivity of a regional climate model to the resolution of the lateral boundary conditions', Climate Dynamics, 20: 107–26.

Devia, Gayathri K, Bigganahalli Puttaswamigowda Ganasri, and Gowdagere Siddaramaiah Dwarakish. 2015. 'A review on hydrological models', Aquatic procedia, 4: 1001–07.

Di Luca, Alejandro, Andrew J Pitman, and Ramón de Elía. 2020. 'Decomposing temperature extremes errors in CMIP5 and CMIP6 models', Geophysical Research Letters, 47: e2020GL088031.

Do, Hong X, Seth Westra, and Michael Leonard. 2017. 'A global-scale investigation of trends in annual maximum streamflow', Journal of Hydrology, 552: 28–43.

ECCC, Environment and Climate Change Canada. 2025. 'ECCC'. https://climate.weather.gc.ca/historical_data/search_historic_data_e.html.

Esteves, Michel. 1996. 'Cartographie d'unités hydrologiques homogènes et modélisation hydrologique, exemple de l'expérience Hapex-Sahel'.

Euser, Tanja, Markus Hrachowitz, Hessel C Winsemius, and Hubert HG Savenije. 2015. 'The effect of forcing and landscape distribution on performance and consistency of model structures', Hydrological Processes, 29: 3727–43.

Fenicia, Fabrizio, Dmitri Kavetski, Hubert HG Savenije, and Laurent Pfister. 2016. 'From spatially variable streamflow to distributed hydrological models: Analysis of key modeling decisions', Water Resources Research, 52: 954–89.

Ficchì, Andrea, Charles Perrin, and Vazken Andréassian. 2019. 'Hydrological modelling at multiple sub-daily time steps: Model improvement via flux-matching', Journal of Hydrology, 575: 1308–27.

Fosser, Giorgia, Marco Gaetani, Elizabeth J Kendon, Marianna Adinolfi, Nikolina Ban, Danijel Belušić, Cécile Caillaud, João AM Careto, Erika Coppola, and Marie-Estelle Demory. 2024. 'Convection-permitting climate models offer more certain extreme rainfall projections', NPJ Climate and atmospheric science, 7: 51.

Fosser, Giorgia, Elizabeth J Kendon, David Stephenson, and Simon Tucker. 2020. 'Convection-permitting models offer promise of more certain extreme rainfall projections', Geophysical Research Letters, 47: e2020GL088151.

Fosser, GSKPB, S Khodayar, and Peter Berg. 2015. 'Benefit of convection permitting climate model simulations in the representation of convective precipitation', Climate Dynamics, 44: 45–60.

García-García, Almudena, Francisco José Cuesta-Valero, Hugo Beltrami, J Fidel González-Rouco, Elena García-Bustamante, and Joel Finnis. 2020. 'Land Surface Model influence on the simulated climatologies of temperature and precipitation extremes in the WRF v. 3.9 model over North America', Geoscientific Model Development Discussions, 2020: 1–29.

Gentry, Megan S, and Gary M Lackmann. 2010. 'Sensitivity of simulated tropical cyclone structure and intensity to horizontal resolution', Monthly Weather Review, 138: 688–704.

Gharari, Shervan, Markus Hrachowitz, F Fenicia, and HHG Savenije. 2011. 'Hydrological landscape classification: investigating the performance of HAND based landscape classifications in a central European meso-scale catchment', Hydrology and Earth System Sciences, 15: 3275–91.

Giordani, Antonio, Ines Maria Luisa Cerenzia, Tiziana Paccagnella, and Silvana Di Sabatino. 2023. 'SPHERA, a new convection-permitting regional reanalysis over Italy: Improving the description of heavy rainfall', Quarterly Journal of the Royal Meteorological Society, 149: 781–808.

Giorgi, Filippo. 2005. 'Climate change prediction', Climatic change, 73: 239–65.

———. 2019. 'Thirty years of regional climate modeling: where are we and where are we going next?', Journal of Geophysical Research: Atmospheres, 124: 5696–723.

Goergen, Klaus, and Stefan Kollet. 2021. 'Boundary condition and oceanic impacts on the atmospheric water balance in limited area climate model ensembles', Scientific reports, 11: 6228.

Grayson, Rodger, and Günter Blöschl. 2001. Spatial patterns in catchment hydrology: observations and modelling (CUP Archive).

Grotch, Stanley L, and Michael C MacCracken. 1991. 'The use of general circulation models to predict regional climatic change', Journal of Climate: 286–303.

Gupta, Hoshin V., Harald Kling, Koray K. Yilmaz, and Guillermo F. Martinez. 2009. 'Decomposition of the mean squared error and NSE performance criteria: Implications for improving hydrological modelling', Journal of Hydrology, 377: 80–91.

Ha, Minh T, Sophie Bastin, Philippe Drobinski, Lluís Fita, Jan Polcher, Olivier Bock, Marjolaine Chiriaco, Danijel Belušić, Cécile Caillaud, and Andreas Dobler. 2024. 'Precipitation frequency in Med-CORDEX and EURO-CORDEX ensembles from 0.44° to convection-permitting resolution: impact of model resolution and convection representation', Climate Dynamics, 62: 4515–40.

Haghnegahdar, Amin, Bryan A Tolson, James R Craig, and Karol T Paya. 2015. 'Assessing the performance of a semi-distributed hydrological model under various watershed discretization schemes', Hydrological Processes, 29: 4018–31.

Hrachowitz, M., and M. P. Clark. 2017a. 'HESS Opinions: The complementary merits of competing modelling philosophies in hydrology', Hydrol. Earth Syst. Sci., 21: 3953–73.

Hrachowitz, Markus, and Martyn P Clark. 2017b. 'HESS Opinions: The complementary merits of competing modelling philosophies in hydrology', Hydrology and Earth System Sciences, 21: 3953–73.

Huet, Maryline, Romain Chesnaux, Marie-Amélie Boucher, and Charles Poirier. 2016. 'Comparing various approaches for assessing groundwater recharge at a regional scale in the Canadian Shield', Hydrological Sciences Journal, 61: 2267–83.

IPCC. 2022. 'IPCC Sixth Assessment Report'. https://www.ipcc.ch/report/ar6/wg2/chapter/chapter-14/?utm_source=chatgpt.com.

Joseph, Jisha, Subimal Ghosh, Amey Pathak, and AK Sahai. 2018. 'Hydrologic impacts of climate change: Comparisons between hydrological parameter uncertainty and climate model uncertainty', Journal of Hydrology, 566: 1–22.

Kay, AL, and MJ Brown. 2023. 'Using sub-daily precipitation for grid-based hydrological modelling across Great Britain: assessing model performance and comparing flood impacts under climate change', Journal of Hydrology: Regional Studies, 50: 101588.

Kay, AL, AC Rudd, HN Davies, EJ Kendon, and RG Jones. 2015. 'Use of very high resolution climate model data for hydrological modelling: baseline performance and future flood changes', Climatic change, 133: 193–208.

Kay, Alison L, Richard G Jones, and Nicholas S Reynard. 2006. 'RCM rainfall for UK flood frequency estimation. II. Climate change results', Journal of Hydrology, 318: 163–72.

Kendon, EJ, Andreas F Prein, CA Senior, and A Stirling. 2021. 'Challenges and outlook for convection-permitting climate modelling', Philosophical Transactions of the Royal Society A, 379: 20190547.

Kendon, Elizabeth J, Nikolina Ban, Nigel M Roberts, Hayley J Fowler, Malcolm J Roberts, Steven C Chan, Jason P Evans, Giorgia Fosser, and Jonathan M Wilkinson. 2017. 'Do convection-permitting regional climate models improve projections of future precipitation change?', Bulletin of the American Meteorological Society, 98: 79–93.

Kendon, Elizabeth J, Nigel M Roberts, Catherine A Senior, and Malcolm J Roberts. 2012. 'Realism of rainfall in a very high-resolution regional climate model', Journal of Climate, 25: 5791–806.

Kienzle, Stefan W. 2008. 'A new temperature based method to separate rain and snow', Hydrological Processes: An International Journal, 22: 5067–85.

Kim, Youngil, Eytan Rocheta, Jason P Evans, and Ashish Sharma. 2020. 'Impact of bias correction of regional climate model boundary conditions on the simulation of precipitation extremes', Climate Dynamics, 55: 3507–26.

Krysanova, Valentina, Chantal Donnelly, Alexander Gelfan, Dieter Gerten, Berit Arheimer, Fred Hattermann, and Zbigniew W Kundzewicz. 2018. 'How the performance of hydrological models relates to credibility of projections under climate change', Hydrological Sciences Journal, 63: 696–720.

Kumar, Rohini, Luis Samaniego, and Sabine Attinger. 2010. 'The effects of spatial discretization and model parameterization on the prediction of extreme runoff characteristics', Journal of Hydrology, 392: 54–69.

Kundzewicz, Zbigniew W, Valentina Krysanova, RE Benestad, Øystein Hov, Mikolaj Piniewski, and Ilona M Otto. 2018. 'Uncertainty in climate change impacts on water resources', Environmental Science & Policy, 79: 1–8.

Lee, Moon-Hwan, Deg-Hyo Bae, and Eun-Soon Im. 2019. 'Effect of the horizontal resolution of climate simulations on the hydrological representation of extreme low and high flows', Water Resources Management, 33: 4653–66.

Lei, Huajin, Hongyi Li, and Wanpin Hu. 2024. 'Enhancing the streamflow simulation of a process-based hydrological model using machine learning and multi-source data', Ecological Informatics, 82: 102755.

Lemaitre-Basset, Thibault, Lila Collet, Guillaume Thirel, Juraj Parajka, Guillaume Evin, and Benoît Hingray. 2021. 'Climate change impact and uncertainty analysis on hydrological extremes in a French Mediterranean catchment', Hydrological Sciences Journal, 66: 888–903.

Leutwyler, David, Daniel Lüthi, Nikolina Ban, Oliver Fuhrer, and Christoph Schär. 2017. 'Evaluation of the convection-resolving climate modeling approach on continental scales', Journal of Geophysical Research: Atmospheres, 122: 5237–58.

Li, Fuyu, Daniele Rosa, William D Collins, and Michael F Wehner. 2012. '"Super-parameterization": A better way to simulate regional extreme precipitation?', Journal of Advances in Modeling Earth Systems, 4.

Li, Jingwan, Jason Evans, Fiona Johnson, and Ashish Sharma. 2017. 'A comparison of methods for estimating climate change impact on design rainfall using a high-resolution RCM', Journal of Hydrology, 547: 413–27.

Li, Lintao, Yanping Li, and Zhenhua Li. 2020. 'Object-based tracking of precipitation systems in western Canada: the importance of temporal resolution of source data', Climate Dynamics, 55: 2421–37.

Liu, Changhai, Kyoko Ikeda, Roy Rasmussen, Mike Barlage, Andrew J Newman, Andreas F Prein, Fei Chen, Liang Chen, Martyn Clark, and Aiguo Dai. 2017. 'Continental-scale convection-permitting modeling of the current and future climate of North America', Climate Dynamics, 49: 71–95.

Llasat, Maria Carmen, Raul Marcos, Marco Turco, Joan Gilabert, and Montserrat Llasat-Botija. 2016. 'Trends in flash flood events versus convective precipitation in the Mediterranean region: The case of Catalonia', Journal of Hydrology, 541: 24–37.

Lucas-Picher, Philippe, Erwan Brisson, Cécile Caillaud, Antoinette Alias, Pierre Nabat, Aude Lemonsu, Nils Poncet, Virginia Edith Cortés Hernandez, Yohanna Michau, and Antoine Doury. 2024. 'Evaluation of the convection-permitting regional climate model CNRM-AROME41t1 over Northwestern Europe', Climate Dynamics, 62: 4587–615.

Lucas-Picher, Philippe, René Laprise, and Katja Winger. 2017. 'Evidence of added value in North American regional climate model hindcast simulations using ever-increasing horizontal resolutions', Climate Dynamics, 48: 2611–33.

Lucas-Picher, Philippe, Daniel Argüeso, Erwan Brisson, Yves Tramblay, Peter Berg, Aude Lemonsu, Sven Kotlarski, and Cécile Caillaud. 2021. 'Convection-permitting modeling with regional climate models: Latest developments and next steps', Wiley Interdisciplinary Reviews: Climate Change, 12: e731.

Lucas-Picher, Philippe, Simon Lachance-Cloutier, Richard Arsenault, Annie Poulin, Simon Ricard, Richard Turcotte, and Francois Brissette. 2021. 'Will Evolving Climate Conditions Increase the Risk of Floods of the Large US-Canada Transboundary

Richelieu River Basin?', JAWRA Journal of the American Water Resources Association, 57: 32–56.

Ludwig, R, I May, R Turcotte, L Vescovi, M Braun, J-F Cyr, L-G Fortin, D Chaumont, S Biner, and I Chartier. 2009. 'The role of hydrological model complexity and uncertainty in climate change impact assessment', Advances in Geosciences, 21: 63–71.

Mai, Juliane. 2023. 'Ten strategies towards successful calibration of environmental models', Journal of Hydrology, 620: 129414.

Mailhot, Alain, Sophie Duchesne, Daniel Caya, and Guillaume Talbot. 2007. 'Assessment of future change in intensity–duration–frequency (IDF) curves for Southern Quebec using the Canadian Regional Climate Model (CRCM)', Journal of Hydrology, 347: 197–210.

Marsham, John H, Nick S Dixon, Luis Garcia-Carreras, Grenville MS Lister, Douglas J Parker, Peter Knippertz, and Cathryn E Birch. 2013. 'The role of moist convection in the West African monsoon system: Insights from continental-scale convection-permitting simulations', Geophysical Research Letters, 40: 1843–49.

Marsigli, C, A Montani, and T Paccagnella. 2014. 'Provision of boundary conditions for a convection-permitting ensemble: comparison of two different approaches', Nonlinear Processes in Geophysics, 21: 393–403.

McGinnis, Seth, and Linda Mearns. 2021. 'Building a climate service for North America based on the NA-CORDEX data archive', Climate Services, 22: 100233.

MELCCFP, River discharge data from. 2025. 'MELCCFP'. https://www.environnement.gouv.qc.ca/.

Meresa, Hadush, Yongqiang Zhang, Jing Tian, Ning Ma, Xuanze Zhang, Hadi Heidari, and Shahid Naeem. 2023. 'An integrated modeling framework in projections of hydrological extremes', Surveys in Geophysics, 44: 277–322.

Moazami, S, and MR Najafi. 2021. 'A comprehensive evaluation of GPM-IMERG V06 and MRMS with hourly ground-based precipitation observations across Canada', Journal of Hydrology, 594: 125929.

Moges, Edom, Yonas Demissie, Laurel Larsen, and Fuad Yassin. 2021. 'Sources of hydrological model uncertainties and advances in their analysis', Water, 13: 28.

Moradkhani, Hamid, and Soroosh Sorooshian. 2009. 'General review of rainfall-runoff modeling: model calibration, data assimilation, and uncertainty analysis', Hydrological modelling and the water cycle: Coupling the atmospheric and hydrological models: 1–24.

Muñoz-Sabater, Joaquín, Emanuel Dutra, Anna Agustí-Panareda, Clément Albergel, Gabriele Arduini, Gianpaolo Balsamo, Souhail Boussetta, Margarita Choulga, Shaun Harrigan, and Hans Hersbach. 2021. 'ERA5-Land: A state-of-the-art global reanalysis dataset for land applications', Earth system science data, 13: 4349–83.

Nazarian, Robert H, James V Vizzard, Carissa P Agostino, and Nicholas J Lutsko. 2022. 'Projected changes in future extreme precipitation over the northeast United States in the NA-CORDEX ensemble', Journal of Applied Meteorology and Climatology, 61: 1649–68.

Nemri, Saida, and Christophe Kinnard. 2020. 'Comparing calibration strategies of a conceptual snow hydrology model and their impact on model performance and parameter identifiability', Journal of Hydrology, 582: 124474.

Oudin, Ludovic, Frédéric Hervieu, Claude Michel, Charles Perrin, Vazken Andréassian, François Anctil, and Cécile Loumagne. 2005. 'Which potential evapotranspiration input for a lumped rainfall–runoff model?: Part 2—Towards a simple and efficient potential evapotranspiration model for rainfall–runoff modelling', Journal of Hydrology, 303: 290–306.

Oudin, Ludovic, Claude Michel, and François Anctil. 2005. 'Which potential evapotranspiration input for a lumped rainfall-runoff model?: Part 1—Can rainfall-runoff models effectively handle detailed potential evapotranspiration inputs?', Journal of Hydrology, 303: 275–89.

Palmer, Tim N. 2019. 'Stochastic weather and climate models', Nature Reviews Physics, 1: 463–71.

Pechlivanidis, IG, B Jackson, H McMillan, and H Gupta. 2014. 'Use of an entropy-based metric in multiobjective calibration to improve model performance', Water Resources Research, 50: 8066–83.

Perrin, Charles, Claude Michel, and Vazken Andréassian. 2003. 'Improvement of a parsimonious model for streamflow simulation', Journal of Hydrology, 279: 275–89.

Piani, Claudio, GP Weedon, M Best, SM Gomes, Pedro Viterbo, Stefan Hagemann, and JO Haerter. 2010. 'Statistical bias correction of global simulated daily precipitation and temperature for the application of hydrological models', Journal of Hydrology, 395: 199–215.

Poncet, Nils, Philippe Lucas-Picher, Yves Tramblay, Guillaume Thirel, Humberto Vergara, Jonathan Gourley, and Antoinette Alias. 2024. 'Does a convection-permitting regional climate model bring new perspectives on the projection of Mediterranean floods?', Natural Hazards and Earth System Sciences, 24: 1163–83.

Prein, Andreas F, Wolfgang Langhans, Giorgia Fosser, Andrew Ferrone, Nikolina Ban, Klaus Goergen, Michael Keller, Merja Tölle, Oliver Gutjahr, and Frauke Feser. 2015. 'A review on regional convection-permitting climate modeling: Demonstrations, prospects, and challenges', Reviews of Geophysics, 53: 323–61.

Qing, Yamin, Shuo Wang, Boen Zhang, and Yonggang Wang. 2020. 'Ultra-high resolution regional climate projections for assessing changes in hydrological extremes and underlying uncertainties', Climate Dynamics, 55: 2031–51.

Raffa, Mario, Alfredo Reder, Marianna Adinolfi, and Paola Mercogliano. 2021. 'A comparison between one-step and two-step nesting strategy in the dynamical downscaling of regional climate model COSMO-CLM at 2.2 km driven by ERA5 reanalysis', Atmosphere, 12: 260.

Rasmussen, Roy M, and Changhai Liu. 2017. 'High resolution WRF simulations of the current and future climate of North America'.

Rendfrey, Tristan S., Melissa S. Bukovsky, Rachel R. McCrary, and Ramón Fuentes-Franco. 2021. 'An assessment of tropical cyclones in North American CORDEX WRF simulations', Weather and Climate Extremes, 34: 100382.

Reszler, Christian, Matthew Blaise Switanek, and Heimo Truhetz. 2018. 'Convection-permitting regional climate simulations for representing floods in small-and medium-sized catchments in the Eastern Alps', Natural Hazards and Earth System Sciences, 18: 2653–74.

Riboust, Philippe, Guillaume Thirel, Nicolas Le Moine, and Pierre Ribstein. 2019. 'Revisiting a simple degree-day model for integrating satellite data: implementation of SWE-SCA hystereses', Journal of hydrology and hydromechanics, 67: 70–81.

Rinsema, Jan Gert. 2014. 'Comparison of rainfall runoff models for the Florentine Catchment', University of Twente.

Rode, Michael, George Arhonditsis, Daniela Balin, Tesfaye Kebede, Valentina Krysanova, Ann Van Griensven, and Sjoerd EATM Van der Zee. 2010. 'New challenges in integrated water quality modelling', Hydrological Processes, 24: 3447–61.

Rousseau, Alain N., Iris M. Klein, Daphné Freudiger, Patrick Gagnon, Anne Frigon, and Claudie Ratté-Fortin. 2014. 'Development of a methodology to evaluate probable maximum precipitation (PMP) under changing climate conditions: Application to southern Quebec, Canada', Journal of Hydrology, 519: 3094–109.

Rummukainen, Markku. 2010. 'State-of-the-art with regional climate models', Wiley Interdisciplinary Reviews: Climate Change, 1: 82–96.

Sabzipour, Behmard, Philippe Lucas-Picher, Richard Turcotte, and Gabriel Rondeau-Genesse. 2025. 'Can high-resolution convection-permitting climate models improve flood simulation in southern Quebec watersheds?', EGUsphere, 2025: 1–39.

Santos, Léonard, Guillaume Thirel, and Charles Perrin. 2018. 'Pitfalls in using log-transformed flows within the KGE criterion', Hydrology and Earth System Sciences, 22: 4583–91.

Schär, Christoph, Oliver Fuhrer, Andrea Arteaga, Nikolina Ban, Christophe Charpilloz, Salvatore Di Girolamo, Laureline Hentgen, Torsten Hoefler, Xavier Lapillonne, and David Leutwyler. 2020. 'Kilometer-scale climate models: Prospects and challenges', Bulletin of the American Meteorological Society, 101: E567–E87.

Seo, Bong-Chul, Felipe Quintero, and Witold F Krajewski. 2023. 'Hydrologic assessment of IMERG products across spatial scales over Iowa', Journal of Hydrometeorology, 24: 997–1015.

Sharma, Ashish, Conrad Wasko, and Dennis P Lettenmaier. 2018. 'If precipitation extremes are increasing, why aren't floods?', Water Resources Research, 54: 8545–51.

Shen, Hongren, Bryan A Tolson, and Juliane Mai. 2022. 'Time to update the split-sample approach in hydrological model calibration', Water Resources Research, 58: e2021WR031523.

Sitterson, Jan, Chris Knightes, Rajbir Parmar, Kurt Wolfe, Brian Avant, and Muluken Muche. 2018. 'An overview of rainfall-runoff model types'.

Su, Jianbin, Haishen Lü, Dongryeol Ryu, and Yonghua Zhu. 2019. 'The assessment and comparison of TMPA and IMERG products over the major basins of Mainland China', Earth and Space Science, 6: 2461–79.

Sun, Qiaohong, Chiyuan Miao, Qingyun Duan, Hamed Ashouri, Soroosh Sorooshian, and Kuo-Lin Hsu. 2018. 'A review of global precipitation data sets: Data sources, estimation, and intercomparisons', Reviews of Geophysics, 56: 79–107.

Tabari, Hossein. 2020. 'Climate change impact on flood and extreme precipitation increases with water availability', Scientific reports, 10: 13768.

Tapiador, Francisco J, Andrés Navarro, Raúl Moreno, José Luis Sánchez, and Eduardo García-Ortega. 2020. 'Regional climate models: 30 years of dynamical downscaling', Atmospheric Research, 235: 104785.

Taylor, Christopher M, Cathryn E Birch, Douglas J Parker, Nick Dixon, Françoise Guichard, Grigory Nikulin, and Grenville MS Lister. 2013. 'Modeling soil moisture-precipitation feedback in the Sahel: Importance of spatial scale versus convective parameterization', Geophysical Research Letters, 40: 6213–18.

Teutschbein, Claudia, and Jan Seibert. 2010. 'Regional climate models for hydrological impact studies at the catchment scale: a review of recent modeling strategies', Geography Compass, 4: 834–60.

Thiboult, Antoine, François Anctil, and Marie-Amélie Boucher. 2016. 'Accounting for three sources of uncertainty in ensemble hydrological forecasting', Hydrology and Earth System Sciences, 20: 1809–25.

Valéry, Audrey. 2010. 'Modélisation précipitations débit sous influence nivale: Elaboration d'un module neige et évaluation sur 380 bassins versants', Doctorat Hydrobiologie, Institut des Sciences et Industries du Vivant et de ….

Vanden Broucke, Sam, Hendrik Wouters, Matthias Demuzere, and Nicole PM van Lipzig. 2019. 'The influence of convection-permitting regional climate modeling on future projections of extreme precipitation: dependency on topography and timescale', Climate Dynamics, 52: 5303–24.

Vogel, Elisabeth, Fiona Johnson, Lucy Marshall, Ulrike Bende-Michl, Louise Wilson, Justin R Peter, Conrad Wasko, Sri Srikanthan, Wendy Sharples, and Andrew Dowdy. 2023. 'An evaluation framework for downscaling and bias correction in climate change impact studies', Journal of Hydrology, 622: 129693.

Wang, Yong, Guang J Zhang, and Yu-Jun He. 2017. 'Simulation of precipitation extremes using a stochastic convective parameterization in the NCAR CAM5 under different resolutions', Journal of Geophysical Research: Atmospheres, 122: 12,875–12,91.

'Weather events 2023'. https://www.canada.ca/en/environment-climate-change/services/top-ten-weather-stories/2023.html?utm_source=chatgpt.com.

'Weather events 2024'. https://www.canada.ca/en/environment-climate-change/services/ten-most-impactful-weather-stories/2024.html.

Wehner, Michael F, Kevin A Reed, Fuyu Li, Prabhat, Julio Bacmeister, Cheng-Ta Chen, Christopher Paciorek, Peter J Gleckler, Kenneth R Sperber, and William D Collins. 2014. 'The effect of horizontal resolution on simulation quality in the C ommunity a tmospheric M odel, CAM 5.1', Journal of Advances in Modeling Earth Systems, 6: 980–97.

Wille, Jonathan D, Rebekka Koch, Tobias Becker, and Erich Fischer. 2025. 'Extreme precipitation depiction in convection-permitting Earth System Models within the nextGEMS project', Journal of Advances in Modeling Earth Systems, 17: e2024MS004840.

Woods, Devon, Pierre-Emmanuel Kirstetter, Humberto Vergara, Jorge A Duarte, and Jeffrey Basara. 2023. 'Hydrologic evaluation of the Global Precipitation Measurement mission over the US: Error budget analysis', Journal of Hydrology, 626: 130212.

Wu, Xiaojing, Jianbin Su, Weiwei Ren, Haishen Lü, and Fei Yuan. 2023. 'Statistical comparison and hydrological utility evaluation of ERA5-Land and IMERG precipitation products on the Tibetan Plateau', Journal of Hydrology, 620: 129384.

Xie, K., L. Li, H. Chen, S. Mayer, A. Dobler, C. Y. Xu, and O. M. Göktürk. 2025. 'Enhanced evaluation of hourly and daily extreme precipitation in Norway from convection-permitting models at regional and local scales', Hydrol. Earth Syst. Sci., 29: 2133–52.

Xie, Kun, Lu Li, Hua Chen, and Chong-Yu Xu. 2025. 'Assessing the performance of convection-permitting climate model in reproducing basin-scale hydrological extremes: A western Norway case study', Journal of Hydrology, 656: 132989.

Zehe, Erwin, Uwe Ehret, Laurent Pfister, Theresa Blume, Boris Schröder, Martijn Westhoff, Conrad Jackisch, Stanislaus J Schymanski, Markus Weiler, and Karsten Schulz. 2014. 'HESS Opinions: From response units to functional units: a thermodynamic reinterpretation of the HRU concept to link spatial organization and functioning of intermediate scale catchments', Hydrology and Earth System Sciences, 18: 4635–55.

Zhang, B, S Wang, and Y Wang. 2021. 'Probabilistic projections of multidimensional flood risks at a convection-permitting scale', Water Resources Research, 57: e2020WR028582.